
Layer-wise Learning of Kernel Dependence Networks

[†]**Chieh Wu**
Northeastern

[†]**Aria Masoomi**
Northeastern

Arthur Gretton
UCL

Jennifer Dy
Northeastern

Abstract

Due to recent debate over the biological plausibility of backpropagation (BP), finding an alternative network optimization strategy has become an active area of interest. We design a new type of kernel network, that is solved greedily, to theoretically answer several questions of interest. First, if BP is difficult to simulate in the brain, are there instead *trivial network weights* (requiring minimum computation) that allow a greedily trained network to classify any pattern. Second, can a greedily trained network converge to a kernel? What kernel will it converge to? Third, is this trivial solution optimal? How is the optimal solution related to generalization? Lastly, can we theoretically identify the network width and depth without a grid search? We prove that the kernel embedding is the trivial solution that compels the greedy procedure to converge to a kernel with Universal property. Yet, this trivial solution is not even optimal. By obtaining the optimal solution spectrally, it provides insight into the generalization of the network while informing us of the network width and depth.[†]

1 Introduction

Due to the brain-inspired architecture of Multi-layered Perceptrons (MLP), the relationship between MLPs and our brains has become a popular topic [1; 2]. This line of research has triggered a controversy [3] around the neural plausibility of backpropagation (BP), i.e., while some contend that brains cannot simulate BP [4; 5], others have recently proposed counterclaims

[†]Signifies equal 1st authorship and contribution.

with a new generation of models [6; 7; 8; 9; 10; 11; 12]. This debate has inspired the search for alternative optimization strategies. Moreover, Strubell et al. [13] have shown that the training of some common AI models can emit over 626,000 pounds of carbon dioxide; this is the carbon footprint 5 times greater than the lifetime usage of a car. Therefore, the environmental impact of BP necessitates a cheaper alternative.

Instead, we should be inspired by the brain’s superior learning capability using only a fraction of the energy. Perhaps artificial neurons can also learn via a simpler path. Among the promising suggestions, a layer-wise strategy has been proposed as a more likely candidate to match existing understandings in Neuroscience [14]. Following this movement, we design a new kernel dependence network (*KNet*) that is solved layer-wise to theoretically answers several questions of interest:

1. Can a network bypass BP to perfectly classify any pattern using only *trivial weights* (W_s)?
2. By greedily stacking more layers, will it converge to a fixed kernel? What kernel exactly is that?
3. Is the trivial solution layer-wise optimal? How is the optimal solution related to generalization?
4. Can we theoretically identify our network width and depth without any grid search?

The 1st question seeks to characterize the potential expressiveness of a network given some *trivial solution*. Perhaps a simple repetition of some basic rule can yield a network equally powerful as ones trained by BP with Stochastic Gradient Descent (SGD). Historically, much work has already been dedicated to identifying MLP’s expressiveness [15; 16; 17; 18; 19]. The *Universal Approximation Theorem* famously claims that a network can approximate any continuous function [15; 16; 20]. While we currently train our network via BP to approach this Universality, our work discovered a much simpler path. Namely, we proved that a network can be optimized to achieve Universality by simply using the kernel embedding (\mathcal{U}) as the *trivial network weight*, a finding that may particularly interest both the kernel and Neuroscience community.

The 2nd question answers how modern MLPs relate to

composition of kernels. The importance of linking kernel methods to neural networks has been emphasized by Belkin and Niyogi [21], and in this respect, work by [22; 23; 24; 14] have analyzed the various composition of kernels. MLPs have also been modeled as a Gaussian process (GP) [25; 26; 27]. This kernel interpretation has inspired a significant amount of research [28; 29; 30; 31]. Extending from the GP perspective, the Neural Tangent Kernel (NTK) has been proposed to describe the dynamics of the network during training [32; 33]. While *KNet* also views the network as a composition of kernels, our model differs in 2 key respects. First, we replace the conventional activation function with the feature map of a Gaussian kernel (GK), resulting in an infinitely wide network that is solved via the kernel trick. Second, instead of using a composition of *fixed* feature maps, we parameterized the GK via a set of linear weights W . This addition yields a model that closely resembles modern MLPs while allowing each layer to actively *choose* the feature map at each layer. We prove that these seemingly minor adjustments are the keys to Universality.

The 3rd question studies the trivial solution, W_s , from an optimization perspective. We will prove that by using W_s to construct each layer, the output of the *final layer* will converge to the global optimum of our objective. However, during the layer-wise construction of each layer, is W_s also a solution where the gradient of the objective is 0? If not, then what is the optimum solution W^* *at each layer*? What is the difference in accuracy between W^* and W_s ? And more importantly, will W^* generalize better than W_s ?

For the question of generalization, it is well known that overparameterized MLPs can generalize even without any explicit regularizer [34]. This observation contradicts classical learning theory and has been a long-standing puzzle [35; 36; 37]. While past works have used the architecture choice and optimization strategies to explain this phenomenon [38; 39; 40], their work cannot be applied to *KNet* due to the difference in architecture and training method. Therefore, *KNet*'s ability to generalize while also being overparameterized raises similar questions. As our second major theoretical contribution, we demonstrate that our architecture and training procedure perform a powerful implicit regularization that grows with the solution, similar to the weight penalization arguments of Poggio et al. [41] for traditional MLPs.

Lastly, we leverage existing work on the network solution landscape [41; 42; 43] to minimize the search space of potential solutions. Specifically, their work suggests that a linear subspace of sufficient dimension is dense enough to represent any solution on the network. They refer to the minimum sufficient dimension

as the *Intrinsic Dimension* (ID). While ID is identifiable experimentally, there has not been much related theoretical work. Our work leverages their finding by constraining our solution space to a linear subspace. In so doing, we are able to identify ID at each layer while relating it to the network width. This constraint, moreover, enables us to solve the network spectrally to identify a solution W^* superior to W_s .

2 Network Model

Let $X \in \mathbb{R}^{n \times d}$ be a dataset of n samples with d features and let $Y \in \mathbb{R}^{n \times \tau}$ be the corresponding one-hot encoded labels with τ number of classes. Let \mathcal{S} be a set of i, j sample pairs that belong to the same class. Its complement, \mathcal{S}^c contains all sample pairs from different classes. Let \odot be the element-wise product. The i^{th} sample and label of the dataset is written as x_i and y_i . H is a centering matrix defined as $H = I_n - \frac{1}{n}\mathbf{1}_n\mathbf{1}_n^T$ where I_n is the identity matrix of size $n \times n$ and $\mathbf{1}_n$ is a vector of 1s also of length n . Given H and the label Y , we let $\Gamma = HYY^TH$.

We denote the MLP weights as $W_1 \in \mathbb{R}^{d \times q}$ and $W_l \in \mathbb{R}^{m \times q}$ for the 1st layer and the l^{th} layer. The input and output at the l^{th} layer are $R_{l-1} \in \mathbb{R}^{n \times m}$ and $R_l \in \mathbb{R}^{n \times m}$, i.e., given $\psi : \mathbb{R}^{n \times q} \rightarrow \mathbb{R}^{n \times m}$ as the activation function, $R_l = \psi(R_{l-1}W_l)$. For each layer, the i^{th} sample/row of its input R_{l-1} is $r_i \in \mathbb{R}^m$. We denote \mathcal{W}_l as a function where $\mathcal{W}_l(R_{l-1}) = R_{l-1}W_l$; consequently, each layer is also a function . By stacking L layers together, the entire network itself becomes a function ϕ where $\phi = \phi_L \circ \dots \circ \phi_1$. Given an empirical risk (\mathcal{H}) and a loss function (\mathcal{L}), our network model assumes an objective of

$$\min_{\phi} \quad \frac{1}{n} \sum_{i=1}^n \mathcal{L}(\phi(x_i), y_i). \quad (1)$$

Notice that *KNet* fundamentally models a traditional MLP where each layer consists of linear weights W_l and an activation function ψ_l . We propose to solve Eq. (1) greedily; this is equivalent to solving a sequence of *single-layered* networks where the previous network output becomes the current layer's input. At each layer, we find the W_l that maximizes the dependency between the layer output and the label via the Hilbert Schmidt Independence Criterion (HSIC) [44]:

$$\begin{aligned} \max_{W_l} \quad & \text{Tr} (\Gamma [\psi(R_{l-1}W_l)\psi^T(R_{l-1}W_l)]) \\ \text{s.t.} \quad & W_l^T W_l = I. \end{aligned} \quad (2)$$

As a major departure of *KNet* from traditional MLPs modeled by past work [22; 23; 24; 14; 25; 26; 27], we generalize the concept of the activation function to a kernel feature map, i.e., while traditional activation

functions are $\psi : \mathbb{R} \rightarrow \mathbb{R}$, we now also include functions that are $\psi : \mathbb{R}^q \rightarrow \mathbb{R}^m$ where m can potentially be ∞ . Specifically, we use the Gaussian kernel (GK) feature map as ψ , simulating an infinitely wide network. Conveniently, HSIC leverages the kernel trick to spare us the direct computation of $\psi(R_{l-1}W_l)\psi^T(R_{l-1}W_l)$; we instead compute

$$\mathcal{K}(W_l^T r_i, W_l^T r_j) = \exp\left\{-\frac{\|W_l^T r_i - W_l^T r_j\|^2}{2\sigma^2}\right\}. \quad (3)$$

The constraint $W^T W = I$ is inspired by the recent work on the geometric landscape of the network solutions [41; 42; 43]. Their work suggests that the network solution can be represented by a linear subspace where only the direction of the weights matter and not the magnitude. If the solution indeed lives on a linear subspace independent of their scale, we can exploit this prior knowledge to narrow the search space during optimization specific to the Stiefel Manifold where $W_l^T W_l = I$, rendering Eq. (2) solvable spectrally.

Why HSIC? Classification tasks can be solved using objectives like Mean Squared Error (MSE) and Cross-Entropy (CE) to match the network output $\phi(X)$ to the label Y . While this approach achieves the desirable outcome, it also constrains the space of potential solutions where $\phi(X)$ must match Y . Yet, if ϕ maps X to the labels $\{0, 1\}$ instead of the true label $\{-1, 1\}$, $\phi(X)$ may not match Y , but the solution is the same. Therefore, enforcing $\phi(X) = Y$ ignores an entire space of solutions that are functionally equivalent. We posit that by relaxing this constraint and accepting a larger space of potential global optima, it will be easier during optimization to collide with this space. This intuition motivates us to depart from the tradition of label matching, and instead seek out alternative objectives that focus on solving the underlying prerequisite of classification, i.e., learning a mapping of X where *similar and different* classes become distinguishable.

However, since there are many notions of *similarity*, it is not always clear which is best for a particular situation. HSIC overcomes this uncertainty by discovering the optimal similarity measure as a kernel function during training. To understand how, first realize that the i, j^{th} element of Γ , denoted as $\Gamma_{i,j}$, is a positive value for samples in \mathcal{S} and negative for \mathcal{S}^c . By defining a kernel \mathcal{K}_{W_l} as a similarity measure between 2 samples where $\mathcal{K}_{W_l} = \langle \phi_l(r_i), \phi_l(r_j) \rangle$, Eq. (2) can also be more intuitively rewritten as

$$\max_{W_l} \sum_{i,j \in \mathcal{S}} \Gamma_{i,j} \mathcal{K}_{W_l}(r_i, r_j) - \sum_{i,j \in \mathcal{S}^c} |\Gamma_{i,j}| \mathcal{K}_{W_l}(r_i, r_j). \quad (4)$$

Understanding HSIC from this non-traditional perspective allows us to see mechanically how HSIC au-

tomatically learns an optimal similarity measure. Notice that the objective uses the sign of $\Gamma_{i,j}$ as labels to guide the choice of W_l such that it increases $\mathcal{K}_{W_l}(r_i, r_j)$ when r_i, r_j belongs to \mathcal{S} while decreasing $\mathcal{K}_{W_l}(r_i, r_j)$ otherwise. Therefore, by finding a W_l matrix that best parameterizes \mathcal{K} , HSIC discovers the optimal kernel \mathcal{K}_{W_l} that separates samples into similar and dissimilar partitions, connecting neural network directly to *kernel discovery*. Following this strategy, we will formally demonstrate how learning \mathcal{K}_{W_l} leads to classification in the coming section.

3 Theoretical Origin

Let the composition of the first l layers as $\phi_l^\circ = \phi_l \circ \dots \circ \phi_1$ where $l \leq L$. This notation enables us to connect the data directly to the layer output where $R_l = \phi_l^\circ(X)$. Since *KNet* is greedy, it solves MLPs by replacing ϕ in Eq. (1) incrementally with a sequence of functions $\{\phi_l^\circ\}_{l=1}^L$ where each layer relies on the output of the previous layer. This implies that we are also solving a sequence of empirical risks $\{\mathcal{H}_l\}_{l=1}^L$, i.e., different versions of Eq. (1). We refer to $\{\phi_l^\circ\}_{l=1}^L$ and $\{\mathcal{H}_l\}_{l=1}^L$ as the *Kernel Sequence* and the *H-Sequence* respectively.

The *H-Sequence* is the central theme of *KNet*. While MLP is traditionally solved with all the layers jointly via BP, *KNet* greedily discovers a *Kernel Sequence* that compels the *H-Sequence* to exhibit key behaviors that enable classification. Specifically, we seek an *H-Sequence* that converges to the global optimum of Eq. (2), i.e., $\mathcal{H}^* = \sum_{i,j \in \mathcal{S}} \Gamma_{i,j}$. To accomplish this, we discovered that the empirical kernel embedding (\mathcal{U}) of each class is the trivial solution W_l for each layer. That is, if we let r_i^j be the i^{th} input sample in class j for layer l , then the trivial solution W_s is

$$W_s = \frac{1}{\sqrt{\zeta}} \begin{bmatrix} \sum_i r_i^{(1)} & \sum_i r_i^{(2)} & \dots & \sum_i r_i^{(\tau)} \end{bmatrix} \quad (5)$$

where ζ is a normalizing constant. Note that since $r_i^j(l) = \phi_l(r_i^j(l-1))$, each column of W_l is the average of all the samples in a single class in RKHS, i.e., the kernel embedding (\mathcal{U}) [45]. Given this definition, we prove in App. A the following theorem.

Theorem 1. *For any \mathcal{H}_0 , there exists a set of bandwidths σ_l and a Kernel Sequence $\{\phi_l^\circ\}_{l=1}^L$ parameterized by $W_l = W_s$ in Eq. (5) such that:*

- I. \mathcal{H}_L can approach arbitrarily close to \mathcal{H}^* such that for any $L > 1$ and $\delta > 0$ we can achieve

$$\mathcal{H}^* - \mathcal{H}_L \leq \delta, \quad (6)$$

- II. as $L \rightarrow \infty$, we have

$$\lim_{L \rightarrow \infty} \mathcal{H}_L = \mathcal{H}^*, \quad (7)$$

III. the convergence is strictly monotonic where

$$\mathcal{H}_l > \mathcal{H}_{l-1} \quad \forall l \geq 1. \quad (8)$$

The theorem identifies the trivial solution W_s and provides an alternative strategy to train a network. Instead of finding the gradient, or needing to propagate information backwards, the global optimum \mathcal{H}^* on training is theoretically possible by choosing the appropriate σ_l at each layer to generate a *H-Sequence* that is monotonically improving toward \mathcal{H}^* . Remember from kernel theory that \mathcal{U}^c embeds the entire distributional information of class c into a single point in RKHS. Therefore, the multiplication of W_s constitutes a projection of each sample onto each class distribution. After this projection, σ_l controls the acceptable pairwise distance between 2 samples of the same class.

To clarify this learning process concretely, given a classification of dogs/cats, the kernel embedding is equivalent to finding the *average* dog/cat. We proved that by iteratively placing Gaussian distributions of size σ_l around these average concepts, perfect classification of any data is possible. While this proof does not claim to have any relationship to the brain, its contribution lies in proving that *simple and repetitive patterns can also achieve perfect classification on any dataset*.

Relating \mathcal{H}^* to Classification. As $\mathcal{H}_l \rightarrow \mathcal{H}^*$, the maximization of Eq. (4) demonstrates how we learn the kernel. However, we have yet to formalize why learning the kernel also enables classification. To clarify this relationship, let us first clarify some key notations and concepts. We refer to the image of ψ and ϕ as the Reproducing Kernel Hilbert Space (RKHS) and the image of \mathcal{W} as the Images of the RKHS Dual Space (IDS). This distinction is crucial because each space dictates the geometric orientations that lead to classification. Consequently, our network can be viewed as a cyclic transition between two spaces as shown in Fig. 1, where each layer constitutes a single cycle.

By modeling MLP layers as a sequence of state transitions, we discovered that the behavior of the entire MLP becomes predictable as *H-Sequence* converges. Keeping this in mind for *KNet*, let us summarize the IDS layer-wise output using the within S_w^l and between S_b^l class scatter matrices defined as

$$\begin{aligned} S_w^l &= \sum_{i,j \in \mathcal{S}} W_l^T (r_i - r_j)(r_i - r_j)^T W_l \\ S_b^l &= \sum_{i,j \in \mathcal{S}^c} W_l^T (r_i - r_j)(r_i - r_j)^T W_l. \end{aligned} \quad (9)$$

These matrices are historically important [46; 47] because their trace ratio $\mathcal{T} = \text{Tr}(S_w)/\text{Tr}(S_b)$ measures

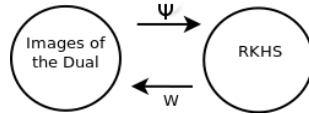


Figure 1: Flow of samples between 2 spaces.

class separability, i.e., a small \mathcal{T} implies a small variance around \mathcal{U} under Euclidean distance. Therefore, a small \mathcal{T} signifies a separation of samples into distinguishable clusters, a crucial criteria for a classifier. In this respect, HSIC is related because we proved that as the cyclic transition pushes $\mathcal{H}_l \rightarrow \mathcal{H}^*$, $\mathcal{T} \rightarrow 0$ as a byproduct. This implies that the *Kernel Sequence* is converging towards ϕ where each class is mapped into its own distinct point apart from each other.

Note that since \mathcal{T} is computed with samples from the image of \mathcal{W} , this particular relationship resides in IDS. Concurrently, since the inner product defines similarity in RKHS, samples are simultaneously being partitioned via the angular distance θ . Indeed, our proof indicates that as $\mathcal{H}_l \rightarrow \mathcal{H}^*$, samples in RKHS within \mathcal{S} achieves perfect alignment ($\theta = 0$) while samples in \mathcal{S}^c become orthogonal to each other, separated by a maximum angle of $\theta = \pi/2$.

This *dual relationship* between IDS and RKHS enables us to predict the outcome of the cyclic transition by designing the network behavior via the kernel selection. For our case, we use the Gaussian kernel to show that *KNet* can employ different notions of distance (Euclidean and angular) to partition and distinguish samples. We formally state these results in the following theorem with the proof in App. C.

Theorem 2. *As $l \rightarrow \infty$ and $\mathcal{H}_l \rightarrow \mathcal{H}^*$, the following properties are satisfied:*

I. the scatter trace ratio \mathcal{T} approaches 0 where

$$\lim_{l \rightarrow \infty} \frac{\text{Tr}(S_w^l)}{\text{Tr}(S_b^l)} = 0 \quad (10)$$

II. the Kernel Sequence converges to the following kernel:

$$\lim_{l \rightarrow \infty} \mathcal{K}(x_i, x_j)^l = \mathcal{K}^*(x_i, x_j)^l = \begin{cases} 0 & \forall i, j \in \mathcal{S}^c \\ 1 & \forall i, j \in \mathcal{S} \end{cases}. \quad (11)$$

As corollaries to Theorem 2, the resulting partition of samples under Euclidean and angular distance implicitly satisfies different classification objectives in each space. In IDS, *KNet* will map a dataset of τ classes into τ distinct points. While these τ points may not match the original label, this difference is inconsequential for classification. In contrast, samples in RKHS at

convergence will reside along τ orthogonal axes on a unit sphere. By realigning these results to the standard bases, solutions that simulate the softmax are generated to solve CE. Therefore, as $\mathcal{H}_l \rightarrow \mathcal{H}^*$, the maximization of Eq. (4) minimizes MSE and CE in different spaces without matching the actual labels itself: instead, we match the underlying geometry of the network output. We state the two corollaries below with their proof in App. F.

Corollary 1. *Given $\mathcal{H}_l \rightarrow \mathcal{H}^*$, the network output in IDS minimizes MSE via a translation of labels.*

Corollary 2. *Given $\mathcal{H}_l \rightarrow \mathcal{H}^*$, the network output in RKHS minimizes CE via a change of bases.*

Optimal Solution of KNet. While a fixed and trivial W_s is interesting as an alternative to BP and SGD, we prove in App. B the following theorem.

Theorem 3. *Given \mathcal{H}_l as the empirical risk at layer $l \neq L$, we have*

$$\frac{\partial}{\partial W_l} \mathcal{H}_l(W_s) \neq 0 \quad (12)$$

From an optimization perspective, it is therefore equally interesting to identify W^* where the gradient is *guaranteed* to be 0, and analyze its properties. Fortunately, this work is already done by Wu et al. [48, 49] with their proposed Iterative Spectral Method (ISM). Applying ISM to our model, each layer’s weight is initialized using the most dominant eigenvectors of

$$Q_{l^0} = R_{l-1}^T (\Gamma - \text{Diag}(\Gamma \mathbf{1}_n)) R_{l-1}, \quad (13)$$

where the $\text{Diag}(\cdot)$ function places the elements of a vector into the diagonal of a square matrix with zero elements. Once the initial weights W_{l^0} are set, ISM iteratively updates W_{l^i} to $W_{l^{i+1}}$ by setting $W_{l^{i+1}}$ to the most dominant eigenvectors of

$$Q_{l^i} = R_{l-1}^T (\hat{\Gamma} - \text{Diag}(\hat{\Gamma} \mathbf{1}_n)) R_{l-1}, \quad (14)$$

where $\hat{\Gamma}$ is a function of W_{l^i} computed with $\hat{\Gamma} = \Gamma \odot K_{R_{l-1} W_{l^i}}$. This iterative weight-updating process stops when $Q_{l^i} \approx Q_{l^{i+1}}$, whereupon $Q_{l^{i+1}}$ is set to Q_l^* , and its most dominant eigenvectors W_l^* becomes the solution of Eq. (2). That is, ISM guarantees that given any σ_l at layer l we have $\frac{\partial}{\partial W_l} \mathcal{H}_l(W_l^*) = 0$.

ISM solves Eq. (2) via the kernel trick directly on an infinitely wide network during training, obtaining W_l^* . Once W_l^* is obtain, we approximate ψ with Random Fourier Features (RFF) [50] to finitely simulate an infinitely wide network and obtain the layer output. This output is then used as input for the next layer.

Learning the Network Width and Depth. Capitalizing on the spectral properties of ISM, the spectrum of Q_l^* automatically determines the dimension of

W_l , i.e., given $W_l^* \in \mathbb{R}^{m \times q}$, the RFF length becomes m , while q is simply the rank of Q_l^* . This is because the eigenvalues of Q_l^* beyond its rank is nearly 0 and their corresponding eigenvectors pose insignificant impact. This insight tells us that the network width is indeed the minimum linear subspace dimension, therefore, the rank of Q_l^* is also the *Intrinsic Dimension* for that layer.

Furthermore, since Eq. (2) after normalization is upper bounded by 1, we can stop adding new layers when the HSIC value of the current layer approaches this theoretical bound, thereby prescribing a natural depth of the network. The resulting network ϕ after training will map samples of the same class into its own cluster, allowing the test samples to be classified by matching their network outputs to the nearest cluster center. The full algorithm is shown in Alg. 1 with its hyperparameters described in the experimental section.

Algorithm 1 KNet Algorithm

```

Input : Data  $X \in \mathbb{R}^{n \times d}$ , Label  $Y \in \mathbb{R}^{n \times \tau}$ 
Output : Network weights  $W_1, \dots, W_L$ 
while  $\mathcal{H}_l < 0.99$  do
    Use the output of last layer as input
    Add a new layer
    Initialize layer weight with Eq. (13)
    while  $Q_{l^i} \not\approx Q_{l^{i+1}}$  do
        | Update  $Q_{l^i} \rightarrow Q_{l^{i+1}}$  with Eq. (14)
    end
     $W_l$  = Most dominant eigenvector of  $Q_l^*$ 
end

```

On Generalization. Besides being an optimum solution, W_l^* exhibit many advantages over W_s . For example, while W_s experimentally generalizes well, ISM identifies W^* faster with even better generalization outcomes. In both cases, the HSIC objective employs an infinitely wide network that should result in overfitting. We ask theoretically, what makes HSIC special? How does ISM contribute to generalization?

Recently, Poggio et al. [41] have proposed that traditional MLPs generalize because gradient methods implicitly regularize the normalized weights. We discovered a similar impact ISM has on HSIC, i.e., the objective can be reformulated to isolate out n functions $[D_1(W_l), \dots, D_n(W_l)]$ that act as a penalty term during optimization. Let S_i be the set of samples that belongs to the i_{th} class and let S_i^c be its complement, then each function $D_i(W_l)$ is defined as

$$\begin{aligned}
 D_i(W_l) = & \frac{1}{\sigma^2} \sum_{j \in S_i} \Gamma_{i,j} \mathcal{K}_{W_l}(r_i, r_j) \\
 & - \frac{1}{\sigma^2} \sum_{j \in S_i^c} |\Gamma_{i,j}| \mathcal{K}_{W_l}(r_i, r_j).
 \end{aligned} \quad (15)$$

Notice that $D_i(W_l)$ is simply Eq. (4) for a single sample scaled by $\frac{1}{\sigma^2}$. Therefore, improving W_l also leads to an increase and decrease of $\mathcal{K}_{W_l}(r_i, r_j)$ associated with \mathcal{S}_i and \mathcal{S}_i^c in Eq. (15), thereby increasing the size of the penalty term $D_i(W_l)$. To appreciate how $D_i(W_l)$ penalizes \mathcal{H} , we propose an equivalent formulation in the theorem below with its derivation in App D.

Theorem 4. *Eq. (4) is equivalent to*

$$\max_{W_l} \sum_{i,j} \frac{\Gamma_{i,j}}{\sigma^2} e^{-\frac{(r_i - r_j)^T W_l W_l^T (r_i - r_j)}{2\sigma^2}} (r_i^T W_l W_l^T r_j) - \sum_i D_i(W_l) \|W_l^T r_i\|_2. \quad (16)$$

Based on Thm. 4, $D_i(W_l)$ adds a negative variable cost to the sample norm in IDS, $\|W_l^T r_i\|_2$, describing how ISM implicitly regularizes HSIC. In fact, a better W_l imposes a heavier penalty on Eq. (16) where the overall \mathcal{H} may actually decrease.

4 Experiments

Datasets. This work focuses on verifying the theoretical claims of *KNet* against traditional MLPs of comparable complexity trained by BP. To isolate out the theory and avoid confounding factors, we used both synthetic and UCI datasets to avoid any kernel approximation. Namely, we use three synthetic (Random, Adversarial and Spiral) and five popular UCI benchmark datasets: wine, cancer, car, divorce, and face [51]. They are included along with the source code in the supplementary, and their comprehensive download link and statistics are in App. G. All theoretical claims are experimentally reproducible with its source code and dataset publicly available at <https://github.com/anonymous>.

Evaluation Metrics. To evaluate the central claim that MLPs can be solved greedily, we report the HSIC objective as \mathcal{H}^* at convergence along with the training/test accuracy for each dataset. Here, \mathcal{H}^* is normalized to the range between 0 to 1 using the method proposed by Cortes et al. [52]. To corroborate Corollaries 1 and 2, we also record MSE and CE. To evaluate the sample geometry predicted by Eq. (10), we recorded the scatter trace ratio \mathcal{T} to measure the compactness of samples within and between classes. The angular distance between samples in \mathcal{S} and \mathcal{S}^c as predicted by Eq. (11) is evaluated with the Cosine Similarity Ratio (C). The equations for \mathcal{H}^* and C are

$$\mathcal{H}^* = \frac{\mathcal{H}(\phi(X), Y)}{\sqrt{\mathcal{H}(\phi(X), \phi(X))\mathcal{H}(Y, Y)}} \quad (17)$$

$$C = \frac{\sum_{i,j \in \mathcal{S}^c} \langle \phi(x_i), \phi(x_j) \rangle}{\sum_{i,j \in \mathcal{S}} \langle \phi(x_i), \phi(x_j) \rangle}. \quad (18)$$

Experiment Settings. The RFF width is set to 300 for all datasets and the σ_l that maximizes HSIC at each layer is chosen (App. L). The convergence threshold for *H-Sequence* is set at $\mathcal{H}_l > 0.99$. The network structures discovered by ISM for every dataset are recorded and provided in App. H. The MLPs that use MSE and CE have weights initialized via the Kaiming method [53]. All datasets are centered to 0 and scaled to a standard deviation of 1. All sources are written in Python using Numpy, Sklearn and Pytorch [54; 55; 56]. All experiments were conducted on an Intel Xeon(R) CPU E5-2630 v3 @ 2.40GHz x 16 with 16 total cores.

Experimental Results. Since Thm. 1 guarantees an optimal convergence for *any* dataset with the sub-optimal W_s , we first designed an Adversarial dataset to trick the network, i.e., the samples pairs in \mathcal{S}^c are intentionally placed significantly closer than samples pairs in \mathcal{S} . We next designed a Random dataset with completely random labels. We then simulated Thm. 1 in Python and plotted the sample behavior in Fig. 2. The original 2-dimensional data is shown next to its 1-dimensional IDS results: each line represents the 1D output at that layer. As predicted by the theorem, the cyclic transitions compel the *H-Sequence* to converge to the global optimum at the 12th layer and perfectly separated the samples based on labels. The experiment confirms our first question that a layer-wise network construction given W_s can also exhibit universal properties.

Using both W_s and W^* , we next conduct 10-fold cross-validation across all 8 datasets and report their mean and the standard deviation for all key metrics in Table 1. Once our model is trained and has learned its structure, we use the same depth and width to train 2 additional MLPs via SGD, where instead of HSIC, MSE and CE are used as the empirical risk.

Can we greedily improve the *H-Sequence*? The \mathcal{H}^* column in Table 1 for ISM consistently reports $\mathcal{H}^* \approx 1$, implying a predictable convergence at its theoretical maximum. Based on Thm. 1 W_s can also reach $\mathcal{H}^* = 1$ as shown in Fig. 2, however in the Table we employed *Early Stopping* to maintain high generalization result, resulting in a lower \mathcal{H}^* value in the Table. Note that a high \mathcal{H}^* is important because Thm. 2 connects HSIC optimization to classification via the cyclic transition outcomes. Therefore, high \mathcal{H}^* should directly translate to a high Training Accuracy. This is confirmed in the Table along the Train Acc column.

While Fig. 2 demonstrates that *KNet* is sufficiently flexible to overfit even random data, will W_s and W^* simply memorize non-random data without any generalization? Since smooth mappings are associated with better generalization, we report the smallest σ use for

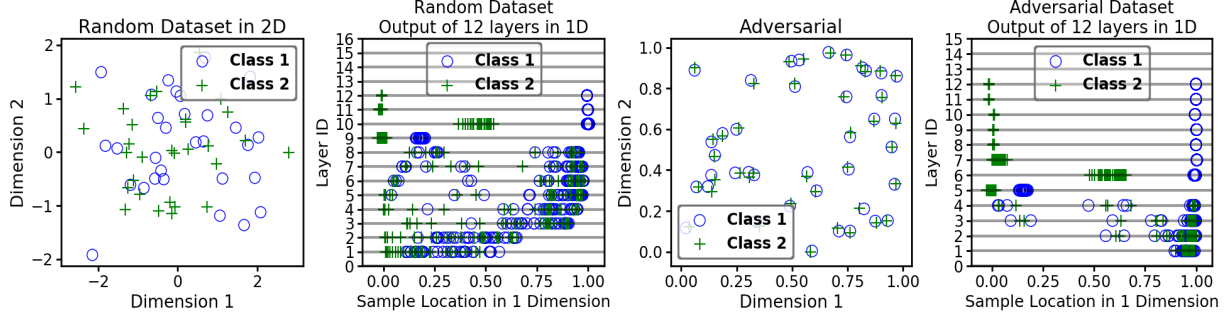


Figure 2: Simulation of Thm. 1 on Random and Adversarial datasets. The 2D representation is shown, and next to it, the 1D output of each layer is displayed over each line. Both datasets achieved the global optimum \mathcal{H}^* at the 12th layers. Refer to App. I for additional results.

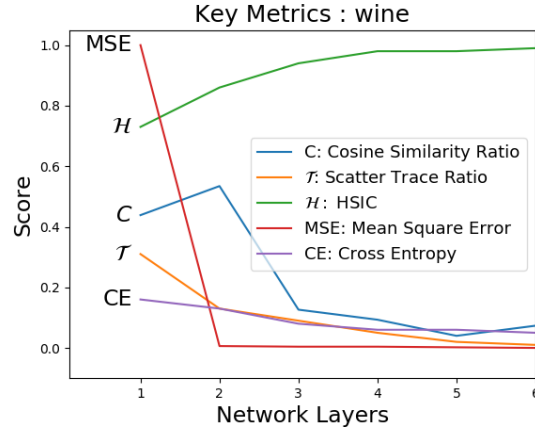


Figure 3: Key evaluation metrics at each layer.

each network to highlight the smoothness of ϕ learned by *KNet*. Correspondingly, with the exception of the two random datasets, the Test Accuracy consistently performed well across all datasets. Therefore, W_s is a *trivial solution that generalizes* given even relatively few data samples. Impressively, ISM performed even better across all datasets. It further differentiates itself on a high dimension Face dataset where it was the only method that avoided overfitting. While we cannot definitively attribute the impressive generalization results of the test dataset to Thm. 4, the experimental evidence appears to be aligned with its implication.

Since Thm. 1 also claims that we can achieve $\mathcal{H}^* - \mathcal{H}_l < \delta$ in *finite* number of layers, we include in Table 1 the average network depth as indicated by length of the \mathcal{H} -Sequence (L). The table suggests that the \mathcal{H} -Sequence using both W_s and W^* converges quickly with 12 layers as the deepest network. Additionally, notice in Fig. 2 where 12 layers are required for the suboptimal W_s to convergence. In contrast, ISM used much smoother and larger σ_s (0.38 and $0.5 \gg 0.15$ and 0.03) and only requires 3 layers to achieve the same result. All of these evidences further suggest that W^*

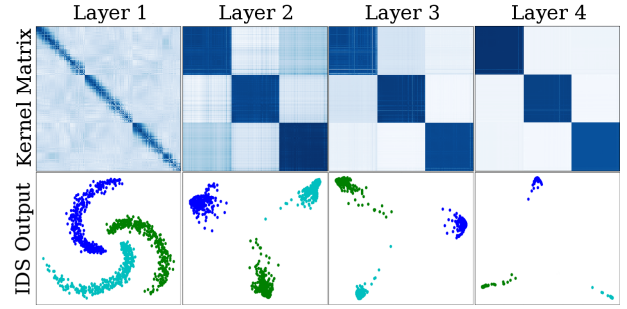


Figure 4: A visual confirmation of Thm. 2. The kernel matrices produced by the *Kernel Sequence* at each layer are displayed in the top row with their corresponding outputs in IDS in the bottom row.

is the superior solution.

The execution time for each objective is also recorded for reference in Table 1. Since *KNet* can be solved via a single forward pass while SGD requires many iterations of BP, *KNet* should be faster. The Time column of Table 1 confirms this expectation by a wide margin. The biggest difference can be observed by comparing the face dataset: ISM finished in 0.78 seconds while MSE required 745 seconds, which is almost a 1000 times difference. Notably, ISM ran even faster than using W_s ; this is because while W_s requires us to perform a grid search of an ideal σ_l , ISM is capable of automatically identifying the optimal σ_l along with W^* . Regardless of this difference, both W_s and W^* trained significantly faster than the traditional MLP using SGD and BP.

Predicted by Thm. 2, *KNet* induces low \mathcal{T} and C as shown in Table 1, implying that samples in \mathcal{S} and \mathcal{S}^c are being pulled together and pushed apart based on Euclidean and angular distance in IDS and RKHS. Given this geometry, will its optimal arguments also induce a low MSE and CE? We evaluate these predictions from Corollaries 1 and 2 by keeping the same net-

	obj	$\sigma \uparrow$	$L \downarrow$	Train Acc \uparrow	Test Acc \uparrow	Time(s) \downarrow	$\mathcal{H}^* \uparrow$	MSE \downarrow	CE \downarrow	$C \downarrow$	$\mathcal{T} \downarrow$
random	ISM	0.38	3.30 \pm 0.64	1.00 \pm 0.00	0.38 \pm 0.21	0.40 \pm 0.37	1.00 \pm 0.01	0.00 \pm 0.01	0.05 \pm 0.00	0.00 \pm 0.06	0.02 \pm 0.0
	W_s	0.15	12 \pm 0.66	0.99 \pm 0.01	0.45 \pm 0.20	0.52 \pm 0.05	0.92 \pm 0.01	2.37 \pm 1.23	0.06 \pm 0.13	0.05 \pm 0.02	0.13 \pm 0.01
	CE	-	3.30 \pm 0.64	1.00 \pm 0.00	0.48 \pm 0.17	25.07 \pm 5.55	1.00 \pm 0.00	10.61 \pm 11.52	0.0 \pm 0.0	0.0 \pm 0.0	0.0 \pm 0.0
	MSE	-	3.30 \pm 0.64	0.98 \pm 0.04	0.63 \pm 0.21	23.58 \pm 8.38	0.93 \pm 0.12	0.02 \pm 0.04	0.74 \pm 0.03	0.04 \pm 0.04	0.08 \pm 0.1
adver	ISM	0.5	3.60 \pm 0.92	1.00 \pm 0.00	0.38 \pm 0.10	0.52 \pm 0.51	1.00 \pm 0.00	0.00 \pm 0.00	0.04 \pm 0.00	0.01 \pm 0.08	0.01 \pm 0.0
	W_s	0.03	12.70 \pm 1.50	0.90 \pm 0.04	0.42 \pm 0.18	2.82 \pm 0.81	0.59 \pm 0.19	15.02 \pm 11.97	0.32 \pm 0.15	0.30 \pm 0.18	0.34 \pm 0.19
	CE	-	3.60 \pm 0.92	0.59 \pm 0.04	0.29 \pm 0.15	69.54 \pm 24.14	0.10 \pm 0.07	0.65 \pm 0.16	0.63 \pm 0.04	0.98 \pm 0.03	0.92 \pm 0.0
	MSE	-	3.60 \pm 0.92	0.56 \pm 0.02	0.32 \pm 0.20	113.75 \pm 21.71	0.02 \pm 0.01	0.24 \pm 0.01	0.70 \pm 0.00	0.99 \pm 0.02	0.95 \pm 0.0
spiral	ISM	0.46	5.10 \pm 0.30	1.00 \pm 0.00	1.00 \pm 0.00	0.87 \pm 0.08	0.98 \pm 0.01	0.01 \pm 0.00	0.02 \pm 0.01	0.04 \pm 0.03	0.02 \pm 0.0
	W_s	0.93	4.00 \pm 1.18	0.99 \pm 0.01	0.96 \pm 0.02	13.54 \pm 5.66	0.88 \pm 0.03	38.60 \pm 25.24	0.06 \pm 0.02	0.08 \pm 0.04	0.08 \pm 0
	CE	-	5.10 \pm 0.30	1.00 \pm 0	1.00 \pm 0	11.59 \pm 5.52	1.00 \pm 0	57.08 \pm 31.25	0 \pm 0	0 \pm 0	0 \pm 0
	MSE	-	5.10 \pm 0.30	1.00 \pm 0	0.99 \pm 0.01	456.77 \pm 78.83	1.00 \pm 0	0 \pm 0	1.11 \pm 0.04	0.40 \pm 0.01	0 \pm 0
wine	ISM	0.47	6.10 \pm 0.54	0.99 \pm 0	0.97 \pm 0.05	0.28 \pm 0.04	0.98 \pm 0.01	0.01 \pm 0	0.07 \pm 0.01	0.04 \pm 0.03	0.02 \pm 0
	W_s	0.98	3.00 \pm 0	0.98 \pm 0.01	0.92 \pm 0.04	0.78 \pm 0.09	0.93 \pm 0.01	2.47 \pm 0.26	0.06 \pm 0.01	0.05 \pm 0.01	0.08 \pm 0.01
	CE	-	6.10 \pm 0.54	1.00 \pm 0.00	0.94 \pm 0.06	3.30 \pm 1.24	1.00 \pm 0.00	40.33 \pm 35.5	0 \pm 0	0 \pm 0	0 \pm 0
	MSE	-	6.10 \pm 0.54	1.00 \pm 0	0.89 \pm 0.17	77.45 \pm 45.40	1.00 \pm 0	0 \pm 0	1.15 \pm 0.07	0.49 \pm 0.02	0 \pm 0
cancer	ISM	0.39	8.10 \pm 0.83	0.99 \pm 0	0.97 \pm 0.02	2.58 \pm 1.07	0.96 \pm 0.01	0.02 \pm 0.01	0.04 \pm 0.01	0.02 \pm 0.04	0.04 \pm 0.0
	W_s	2.33	1.30 \pm 0.46	0.98 \pm 0.01	0.96 \pm 0.03	6.21 \pm 0.36	0.88 \pm 0.01	41.31 \pm 56.17	0.09 \pm 0.01	0.09 \pm 0.02	0.16 \pm 0.03
	CE	-	8.10 \pm 0.83	1.00 \pm 0	0.97 \pm 0.01	82.03 \pm 35.15	1.00 \pm 0	2330 \pm 2915	0 \pm 0	0 \pm 0	0 \pm 0
	MSE	-	8.10 \pm 0.83	1.00 \pm 0.00	0.97 \pm 0.03	151.81 \pm 27.27	1.00 \pm 0	0 \pm 0	0.66 \pm 0.06	0 \pm 0	0 \pm 0
car	ISM	0.23	4.90 \pm 0.30	1.00 \pm 0	1.00 \pm 0.01	1.51 \pm 0.35	0.99 \pm 0	0 \pm 0	0.01 \pm 0.00	0.04 \pm 0.03	0.01 \pm 0
	W_s	1.56	2.70 \pm 0.46	1.00 \pm 0	1.00 \pm 0	5.15 \pm 1.07	0.93 \pm 0.02	12.89 \pm 2.05	0 \pm 0	0.06 \pm 0.02	0.08 \pm 0.02
	CE	-	4.90 \pm 0.30	1.00 \pm 0	1.00 \pm 0	25.79 \pm 18.86	1.00 \pm 0	225.11 \pm 253	0 \pm 0	0 \pm 0	0 \pm 0
	MSE	-	4.90 \pm 0.30	1.00 \pm 0	0.92 \pm 0.10	504 \pm 116.6	1.00 \pm 0	0 \pm 0	1.12 \pm 0.07	0.40 \pm 0	0 \pm 0
face	ISM	0.44	4.00 \pm 0	1.00 \pm 0	0.99 \pm 0.01	0.78 \pm 0.08	0.97 \pm 0	0 \pm 0	0.17 \pm 0	0.01 \pm 0	0 \pm 0
	W_s	0.05	3.40 \pm 0.66	0.97 \pm 0.01	0.80 \pm 0.26	11.12 \pm 3.05	0.86 \pm 0.04	2.07 \pm 1.04	0.28 \pm 0.51	0.04 \pm 0.01	0.01 \pm 0
	CE	-	4.00 \pm 0	1.00 \pm 0	0.79 \pm 0.31	23.70 \pm 8.85	1.00 \pm 0	16099 \pm 16330	0 \pm 0	0 \pm 0	0 \pm 0
	MSE	-	4.00 \pm 0	0.92 \pm 0.10	0.52 \pm 0.26	745.2 \pm 282	0.94 \pm 0.07	0.11 \pm 0.12	3.50 \pm 0.28	0.72 \pm 0.01	0 \pm 0
divorce	ISM	0.41	4.10 \pm 0.54	0.99 \pm 0.01	0.98 \pm 0.02	0.71 \pm 0.41	0.99 \pm 0.01	0.01 \pm 0.01	0.03 \pm 0	0 \pm 0.05	0.02 \pm 0
	W_s	2.10	2.30 \pm 0.64	0.99 \pm 0	0.95 \pm 0.06	1.54 \pm 0.13	0.91 \pm 0.01	60.17 \pm 70.64	0.04 \pm 0.01	0.05 \pm 0.01	0.08 \pm 0
	CE	-	4.10 \pm 0.54	1.00 \pm 0	0.99 \pm 0.02	2.62 \pm 1.21	1.00 \pm 0	14.11 \pm 12.32	0 \pm 0	0 \pm 0	0 \pm 0
	MSE	-	4.10 \pm 0.54	1.00 \pm 0	0.97 \pm 0.03	47.89 \pm 24.31	1.00 \pm 0	0 \pm 0	0.73 \pm 0.07	0 \pm 0.01	0.01 \pm 0

Table 1: Each dataset contains 4 rows comparing the greedily trained *KNet* using ISM and W_s against traditional MLPs trained using MSE and CE via SGD given the same network width and depth. The best results are in bold with \uparrow / \downarrow indicating larger/smaller values preferred.

work weights while replacing the final objective with MSE and CE. Our corroborating results are highlighted in the columns of MSE and CE in Table 1. Interestingly, while using HSIC induces a low MSE and CE, training via BP using either MSE or CE does not necessarily translate to good results for the other.

Fig. 3 plots out all key metrics during training *at each layer*. Here, the *H-Sequence* is clearly monotonic and converging towards a global optimal of 1. Moreover, the trends for \mathcal{T} and C indicate an incremental clustering of samples into separate partitions. Corresponding to low \mathcal{T} and C values, the low MSE and CE errors at convergence further reinforces the claims of Corollaries 1 and 2. This experiment indicates that the *behavior of a layer-wise MLP is predictable* via the cyclic transition model. In fact, these repeatable patterns manifest itself across all datasets as shown in App. K.

We lastly highlight a visual pattern for the *Kernel Sequence* in Fig. 4. We rearrange the samples of the same class to be adjacent to each other. This allows us to quickly evaluate the kernel quality via its block diagonal structure. Since GK is restricted to values between 0 and 1, we let white and dark blue be 0 and 1 respectively where the gradients reflect values in between. Our proof predicts that the *Kernel Se-*

quence should converge to the optimal kernel \mathcal{K}^* , i.e., the *Kernel Sequence* should evolve from an uninformative kernel into a highly discriminating kernel of perfect *block diagonal structures*. Corresponding to the top row, the bottom row plots out the samples in IDS at each layer. As predicted by Thm. 2, the samples of the same class incrementally converge towards a single point in IDS. Indeed, a layer-wise construct *does converge to a kernel* and it converges to an optimal kernel \mathcal{K}^* . Again, this pattern is observable on all datasets, and the complete collection of the *kernel sequences* for each dataset can be found in App. J.

Conclusion. We have presented a new model of MLP for classification using either W_s or W^* while bypassing BP and SGD. Due to the trivial computation requirement of W_s , this solution proves the possibility that networks (potentially the brain) can classify any data using only a repetition of simple patterns. The resulting geometric orientation of the samples minimizes the scatter ratio while produces an optimal kernel, \mathcal{K}^* , resulting in a geometric orientation that consequently solves MSE and CE in different spaces. These patterns are predictable by our theorems and experimentally reproducible. Therefore, we hope that *KNet* opens the door to a new perspective to analyze MLPs.

We thank all reviewers for the supportive comments on our novel network model that bypasses backpropagation. We are encouraged that every reviewer found our analysis correct and reproducible. We are excited that R3 and R7 recognize our model as a novel way to analyze and predict network behaviors and acknowledges the importance of this topic. We appreciate R2 recognizing the potential impact of this work. You are correct that this work is motivated by returning to the biological roots and finding an alternative network optimization approach that better mimics the brain. Like you, the authors were also surprised and impressed by how a simple and recursive greedy approach can rival backpropagation and SGD. Lastly, we thank R1 for identifying some related work that deserves more attention; your valuable suggestions will be incorporated into the camera-ready version.

R1. Thank you for suggesting the additional related work. Our work is related because our formulation is also implemented with a deep kernel structure. Our work is different because our contribution focuses on finding a brain-inspired greedy approach that optimizes a network without backpropagation and SGD. Note that none of the recommended work is greedily trained and of all of them used backpropagation or SGD. While the focus is different, we are grateful to R1 for recommending this connection to deep kernel learning. We will clarify this connection and difference in the related work and perform additional experiments based on your recommendations.

Regarding your question on how overfitting is controlled, we proved in the paper that the optimal solution identified by ISM (W^*) produces a strong regularizer, as shown in Eq. (16). This insight is further confirmed experimentally in Table 1, given the highly accurate generalization results.

R2. We thank you for the kind words and the recognition of our work’s impact. We also view KNet as a novel direction to analyze deep learning models. Unlike the Gaussian Process network model, our work suggests that deep network behavior becomes predictable by modeling it as a converging sequence of kernel feature maps. Like you, we also believe this finding will lead to novel learning strategies in the future. Moreover, your instinct on our method’s link to metric learning is reasonable. Indeed, by learning W_l at each layer, we recursively learn a new metric via $(x_i - x_j)^T W_l W_l^T (x_i - x_j)$ for the Gaussian kernel.

R3. Your have insightfully identified the theoretical origin of this work. The interplay between IDS and RKHS suggest that MLPs (when trained greedily) can be analyzed as a converging sequence, making the network behavior predictable by analyzing how and where it converges. We thank you for the suggestion of adding more clarity and detail on this matter; we are happy to provide additional insight into this background in the paper.

Regarding your question on when a linear subspace is sufficient, it was first proposed by Li et al. [42]. Their experiments suggest that a linear subspace may be sufficiently dense to represent all solutions outside of linear subspace. Later, Poggio et al. [41] proved that when the objective is exponential in nature (like our HSIC objective), the solution becomes scale-invariant. Fort et al.[43] experimentally found that the network solution landscape may be spherical in nature. We put these 3 works together and hypothesized that the network solution might lie on a Stiefel Manifold (Spherical, linear subspace, and unit normed.) We confirmed the hypothesis and identified a theoretical justification for the Stiefel Manifold constraint on KNet. Note that when the layer input r_i is multiplied by the weight w_l , this is an inner product inside the RKHS of a Gaussian kernel. Given ϕ as the previous layer, we have

$$r_i = \phi(r_{i-1}) \implies \langle r_i, w_l \rangle = f_w(r_{i-1}) \implies f_w \in \mathcal{F}, \text{RKHS of a Gaussian kernel.} \quad (19)$$

Since the Gaussian kernel is universal with *unit norm* functions in its RKHS, constraining W to the unit norm where $W^T W = I$ yields a function class \mathcal{F} that can fit the shape of any continuous bounded function up to a *scaled factor*. While this scaled difference would not work for regression, classification’s decision boundaries are scaled invariant. Therefore, for classification, the unit norm is sufficient.

R7. Thank you for the suggestion. We are happy to update the bold subtitles to a more visually pleasing spacing. We will also update the 2 typos based on your recommendation.

Regarding your question on references [41] to [43], as discussed with R3 in lines 28 to 32, they are not alternative network models that require any comparison. Instead, their work acts as clues that challenged us to identify a theoretical justification for constraining the solution space. We were able to overcome the challenge via Eq. (1), as discussed with R3. We thank you for bringing to our attention this potential point of confusion; we will better clarify this point in the paper.

References

- [1] Anthony M Zador. A critique of pure learning and what artificial neural networks can learn from animal brains. *Nature communications*, 10(1):1–7, 2019.
- [2] Edgar Y Walker. Deep neural networks uncover what the brain likes to see. *Nature Neuroscience*, 10(1):1–7, 2019.
- [3] James CR Whittington and Rafal Bogacz. Theories of error back-propagation in the brain. *Trends in cognitive sciences*, 2019.
- [4] Francis Crick. The recent excitement about neural networks. *Nature*, 337(6203):129–132, 1989.
- [5] Stephen Grossberg. Competitive learning: From interactive activation to adaptive resonance. *Cognitive science*, 11(1):23–63, 1987.
- [6] Geoffrey Hinton. How to do backpropagation in a brain. In *Invited talk at the NIPS’2007 deep learning workshop*, volume 656, 2007.
- [7] T.P. Lillicrap, A. Santoro, L. Marris, C. Akerman, and G. Hinton. Backpropagation and the brain. In *Nat Rev Neurosci (2020)*, volume 656, 2007.
- [8] Qianli Liao, Joel Z Leibo, and Tomaso Poggio. How important is weight symmetry in backpropagation? In *Thirtieth AAAI Conference on Artificial Intelligence*, 2016.
- [9] Yoshua Bengio, Thomas Mesnard, Asia Fischer, Saizheng Zhang, and Yuhuai Wu. Stdp-compatible approximation of backpropagation in an energy-based model. *Neural computation*, 29(3):555–577, 2017.
- [10] Jordan Guerguiev, Timothy P Lillicrap, and Blake A Richards. Towards deep learning with segregated dendrites. *Elife*, 6:e22901, 2017.
- [11] João Sacramento, Rui Ponte Costa, Yoshua Bengio, and Walter Senn. Dendritic cortical microcircuits approximate the backpropagation algorithm. In *Advances in Neural Information Processing Systems*, pages 8721–8732, 2018.
- [12] James CR Whittington and Rafal Bogacz. An approximation of the error backpropagation algorithm in a predictive coding network with local hebbian synaptic plasticity. *Neural computation*, 29(5):1229–1262, 2017.
- [13] Emma Strubell, Ananya Ganesh, and Andrew McCallum. Energy and policy considerations for deep learning in nlp. *ACL*, 2019.
- [14] Wan-Duo Kurt Ma, JP Lewis, and W Bastiaan Kleijn. The hsic bottleneck: Deep learning without back-propagation. *AAAI*, 2019.
- [15] George Cybenko. Approximation by superpositions of a sigmoidal function. *Mathematics of control, signals and systems*, 2(4):303–314, 1989.
- [16] Kurt Hornik. Approximation capabilities of multilayer feedforward networks. *Neural networks*, 4(2):251–257, 1991.
- [17] Zhou Lu, Hongming Pu, Feicheng Wang, Zhiqiang Hu, and Liwei Wang. The expressive power of neural networks: A view from the width. In *Advances in neural information processing systems*, pages 6231–6239, 2017.
- [18] Guido F Montufar, Razvan Pascanu, Kyunghyun Cho, and Yoshua Bengio. On the number of linear regions of deep neural networks. In *Advances in neural information processing systems*, pages 2924–2932, 2014.
- [19] Ben Poole, Subhaneil Lahiri, Maithra Raghu, Jascha Sohl-Dickstein, and Surya Ganguli. Exponential expressivity in deep neural networks through transient chaos. In *Advances in neural information processing systems*, pages 3360–3368, 2016.
- [20] Ding-Xuan Zhou. Universality of deep convolutional neural networks. *Applied and computational harmonic analysis*, 48(2):787–794, 2020.
- [21] Mikhail Belkin and Partha Niyogi. Laplacian eigenmaps for dimensionality reduction and data representation. *Neural computation*, 15(6):1373–1396, 2003.
- [22] Julien Mairal, Piotr Koniusz, Zaid Harchaoui, and Cordelia Schmid. Convolutional kernel networks. In *Advances in neural information processing systems*, pages 2627–2635, 2014.

- [23] Jinfeng Zhuang, Ivor W Tsang, and Steven CH Hoi. Two-layer multiple kernel learning. In *Proceedings of the Fourteenth International Conference on Artificial Intelligence and Statistics*, pages 909–917, 2011.
- [24] Grasgoire Montavon, Mikio L Braun, and Klaus-Robert Müller. Kernel analysis of deep networks. *Journal of Machine Learning Research*, 12(Sep):2563–2581, 2011.
- [25] Radford M Neal. *Bayesian learning for neural networks*, volume 118. Springer Science & Business Media, 2012.
- [26] Alexander G de G Matthews, Mark Rowland, Jiri Hron, Richard E Turner, and Zoubin Ghahramani. Gaussian process behaviour in wide deep neural networks. *ICLR*, 2018.
- [27] Jaehoon Lee, Yasaman Bahri, Roman Novak, Samuel S Schoenholz, Jeffrey Pennington, and Jascha Sohl-Dickstein. Deep neural networks as gaussian processes. *ICLR*, 2017.
- [28] Soufiane Hayou, Arnaud Doucet, and Judith Rousseau. On the impact of the activation function on deep neural networks training. *ICML*, 2019.
- [29] Jaehoon Lee, Lechao Xiao, Samuel S Schoenholz, Yasaman Bahri, Jascha Sohl-Dickstein, and Jeffrey Pennington. Wide neural networks of any depth evolve as linear models under gradient descent. *NeurIPS*, 2019.
- [30] Greg Yang. Scaling limits of wide neural networks with weight sharing: Gaussian process behavior, gradient independence, and neural tangent kernel derivation. *arXiv preprint arXiv:1902.04760*, 2019.
- [31] David Duvenaud, Oren Rippel, Ryan Adams, and Zoubin Ghahramani. Avoiding pathologies in very deep networks. In *Artificial Intelligence and Statistics*, pages 202–210, 2014.
- [32] Arthur Jacot, Franck Gabriel, and Clément Hongler. Neural tangent kernel: Convergence and generalization in neural networks. In *Advances in neural information processing systems*, pages 8571–8580, 2018.
- [33] Sanjeev Arora, Simon S Du, Wei Hu, Zhiyuan Li, Ruslan Salakhutdinov, and Ruosong Wang. On exact computation with an infinitely wide neural net. *NeurIPS*, 2019.
- [34] C. Zhang, S. Bengio, M. Hardt, B. Recht, and Oriol Vinyals. Understanding deep learning requires rethinking generalization. *ICLR*, abs/1611.03530, 2017.
- [35] Yuan Cao and Quanquan Gu. Generalization bounds of stochastic gradient descent for wide and deep neural networks. In *Advances in Neural Information Processing Systems*, pages 10835–10845, 2019.
- [36] Alon Brutzkus, Amir Globerson, Eran Malach, and Shai Shalev-Shwartz. Sgd learns over-parameterized networks that provably generalize on linearly separable data. *ICLR*, 2017.
- [37] Zeyuan Allen-Zhu, Yuanzhi Li, and Yingyu Liang. Learning and generalization in overparameterized neural networks, going beyond two layers. In *Advances in neural information processing systems*, pages 6155–6166, 2019.
- [38] Devansh Arpit, Stanislaw Jastrzebski, Nicolas Ballas, David Krueger, Emmanuel Bengio, Maxinder S Kanwal, Tegan Maharaj, Asja Fischer, Aaron Courville, Yoshua Bengio, et al. A closer look at memorization in deep networks. In *Proceedings of the 34th International Conference on Machine Learning-Volume 70*, pages 233–242. JMLR.org, 2017.
- [39] Giacomo De Palma, Bobak Kiani, and Seth Lloyd. Random deep neural networks are biased towards simple functions. In *Advances in Neural Information Processing Systems*, pages 1962–1974, 2019.
- [40] Guillermo Valle-Pérez, Chico Q Camargo, and Ard A Louis. Deep learning generalizes because the parameter-function map is biased towards simple functions. *ICLR*, 2018.
- [41] Tomaso Poggio, Qianli Liao, and Andrzej Banburski. Complexity control by gradient descent in deep networks. *Nature Communications*, 11(1):1–5, 2020.
- [42] Chunyuan Li, Heerad Farkhoor, Rosanne Liu, and Jason Yosinski. Measuring the intrinsic dimension of objective landscapes. *ICLR*, 2018.
- [43] Stanislav Fort and Stanislaw Jastrzebski. Large scale structure of neural network loss landscapes. In *NeurIPS*, 2019.
- [44] Arthur Gretton, Olivier Bousquet, Alex Smola, and Bernhard Schölkopf. Measuring statistical dependence with hilbert-schmidt norms. In *International conference on algorithmic learning theory*, pages 63–77. Springer, 2005.

- [45] Krikamol Muandet, Kenji Fukumizu, Bharath Sriperumbudur, and Bernhard Schölkopf. Kernel mean embedding of distributions: A review and beyond. *arXiv preprint arXiv:1605.09522*, 2016.
- [46] Ronald A Fisher. The use of multiple measurements in taxonomic problems. *Annals of eugenics*, 7(2):179–188, 1936.
- [47] Geoffrey J McLachlan. *Discriminant analysis and statistical pattern recognition*, volume 544. John Wiley & Sons, 2004.
- [48] Chieh Wu, Stratis Ioannidis, Mario Sznaier, Xiangyu Li, David Kaeli, and Jennifer Dy. Iterative spectral method for alternative clustering. In *International Conference on Artificial Intelligence and Statistics*, pages 115–123, 2018.
- [49] Chieh T Wu, J. Miller, Y. Chang, M. Sznaier, and Jennifer G. Dy. Solving interpretable kernel dimensionality reduction. In *NeurIPS*, 2019.
- [50] Ali Rahimi and Benjamin Recht. Random features for large-scale kernel machines. In *Advances in neural information processing systems*, pages 1177–1184, 2008.
- [51] Dua Dheeru and Efi Karra Taniskidou. UCI machine learning repository, 2017. URL <http://archive.ics.uci.edu/ml>.
- [52] Corinna Cortes, Mehryar Mohri, and Afshin Rostamizadeh. Algorithms for learning kernels based on centered alignment. *Journal of Machine Learning Research*, 13(Mar):795–828, 2012.
- [53] Kaiming He, Xiangyu Zhang, Shaoqing Ren, and Jian Sun. Delving deep into rectifiers: Surpassing human-level performance on imagenet classification. In *Proceedings of the IEEE international conference on computer vision*, pages 1026–1034, 2015.
- [54] Eric Jones, Travis Oliphant, Pearu Peterson, et al. SciPy: Open source scientific tools for Python, 2001–. URL <http://www.scipy.org/>. [Online; accessed 1today].
- [55] Lars Buitinck, Gilles Louppe, Mathieu Blondel, Fabian Pedregosa, Andreas Mueller, Olivier Grisel, Vlad Niculae, Peter Prettenhofer, Alexandre Gramfort, Jaques Grobler, Robert Layton, Jake VanderPlas, Arnaud Joly, Brian Holt, and Gaël Varoquaux. API design for machine learning software: experiences from the scikit-learn project. In *ECML PKDD Workshop: Languages for Data Mining and Machine Learning*, pages 108–122, 2013.
- [56] Adam Paszke, Sam Gross, Soumith Chintala, Gregory Chanan, Edward Yang, Zachary DeVito, Zeming Lin, Alban Desmaison, Luca Antiga, and Adam Lerer. Automatic differentiation in pytorch. 2017.
- [57] Alessio Ansuini, Alessandro Laio, Jakob H Macke, and Davide Zoccolan. Intrinsic dimension of data representations in deep neural networks. *NeurIPS*, 2019.

Appendix A Proof for Theorem 1

Theorem 1: For any \mathcal{H}_0 , there exists a set of bandwidths σ_l and a Kernel Sequence $\{\phi_l\}_{l=1}^L$ parameterized by $W_l = W_s$ in Eq. (5) such that:

- I. \mathcal{H}_L can approach arbitrarily close to \mathcal{H}^* such that for any $L > 1$ and $\delta > 0$ we can achieve

$$\mathcal{H}^* - \mathcal{H}_L \leq \delta, \quad (20)$$

- II. as $L \rightarrow \infty$, the \mathcal{H} -Sequence converges to the global optimum, that is

$$\lim_{L \rightarrow \infty} \mathcal{H}_L = \mathcal{H}^*, \quad (21)$$

- III. the convergence is monotonic where

$$\mathcal{H}_l > \mathcal{H}_{l-1} \quad \forall l. \quad (22)$$

Lemma 1. Given σ_0 and σ_1 as the σ values from the last layer and the current layer, then there exists a lower bound for \mathcal{H}_l , denoted as $\mathcal{L}(\sigma_0, \sigma_1)$ such that

$$\mathcal{H}_l \geq \mathcal{L}(\sigma_0, \sigma_1). \quad (23)$$

Basic Background, Assumptions, and Notations.

1. The simulation of this theorem for Adversarial and Random data is also publicly available on <https://github.com/anonymous>.
2. Here we show that this bound can be established given the last 2 layers.
3. σ_0 is the σ value of the previous layer
4. σ_1 is the σ value of the current layer
5. τ is the number of classes
6. n is total number of samples
7. n_i is number of samples in the i^{th} class
8. \mathcal{S} is a set of all i, j sample pairs where r_i and r_j belong to the same class.
9. \mathcal{S}^c is a set of all i, j sample pairs where r_i and r_j belong to different same classes.
10. \mathcal{S}^β is a set of all i, j sample pairs that belongs to the same β^{th} classes.
11. $r_i^{(\alpha)}$ is the i^{th} sample in the α^{th} class among τ classes.
12. We assume no $r_i \neq r_j$ pair are equal $\forall i \neq j$.
13. Among all $r_i \neq r_j$ pairs, there exists an optimal r_i^*, r_j^* pair where $\langle r_i^*, r_j^* \rangle \geq \langle r_i, r_j \rangle \forall r_i \neq r_i^* \text{ and } r_j \neq r_j^*$. We denote this maximum inner product as

$$u_{\sigma_0} = \langle r_i^*, r_j^* \rangle. \quad (24)$$

14. In *KNet*, each r_i sample is assumed to be a sample in the RKHS of the Gaussian kernel, therefore all inner products are bounded such that

$$0 \leq \langle r_i, r_j \rangle \leq u_{\sigma_0}. \quad (25)$$

15. We let W be

$$W_s = \frac{1}{\sqrt{\zeta}} \begin{bmatrix} \sum_i r_i^{(1)} & \sum_i r_i^{(2)} & \dots & \sum_i r_i^{(\tau)} \end{bmatrix}. \quad (26)$$

Instead of using an optimal W^* defined as $W^* = \arg \max_W H_l(W)$, we use a suboptimal W_s where each dimension is simply the average direction of each class: $\frac{1}{\sqrt{\zeta}}$ is a normalizing constant $\zeta = \|W_s\|_2^2$ that ensures $W_s^T W_s = I$. By using W_s , this implies that the \mathcal{H} we obtain is already a lower bound compare \mathcal{H} obtained by W^* . But, we will use this suboptimal W_s to identify an even lower bound. Note that based on the definition W^* , we have the property $\mathcal{H}(W^*) \geq \mathcal{H}(W) \forall W$.

16. We note that the objective \mathcal{H} is

$$\mathcal{H} = \underbrace{\sum_{i,j \in \mathcal{S}} \Gamma_{i,j} e^{-\frac{(r_i - r_j)^T W W^T (r_i - r_j)}{2\sigma_1^2}}}_{\mathcal{W}} - \underbrace{\sum_{i,j \in \mathcal{S}^c} |\Gamma_{i,j}| e^{-\frac{(r_i - r_j)^T W W^T (r_i - r_j)}{2\sigma_1^2}}}_{\mathcal{B}} \quad (27)$$

where we let \mathcal{W} be the summation of terms associated with the within cluster pairs, and let \mathcal{B} be the summation of terms associated with the between cluster pairs.

Proof.

The equation is divided into smaller parts organized into multiple sections.

For sample pairs in \mathcal{S} . The first portion of the function can be split into multiple classes where

$$\mathcal{W} = \underbrace{\sum_{\mathcal{S}^1} \Gamma_{i,j} e^{-\frac{(r_i^{(1)} - r_j^{(1)})^T W W^T (r_i^{(1)} - r_j^{(1)})}{2\sigma_1^2}}}_{\mathcal{W}_1} + \dots + \underbrace{\sum_{\mathcal{S}^\tau} \Gamma_{i,j} e^{-\frac{(r_i^{(\tau)} - r_j^{(\tau)})^T W W^T (r_i^{(\tau)} - r_j^{(\tau)})}{2\sigma_1^2}}}_{\mathcal{W}_\tau} \quad (28)$$

Realize that to find the lower bound, we need to determine the minimum possible value of each term which translates to **maximum** possible value of each exponent. Without loss of generality we can find the lower bound for one term and generalize its results to other terms due to their similarity. Let us focus on the numerator of the exponent from \mathcal{W}_1 . Given W_s as W , our goal is identify the **maximum** possible value for

$$\underbrace{(r_i^{(1)} - r_j^{(1)})^T W}_{\Pi_1} \underbrace{W^T (r_i^{(1)} - r_j^{(1)})}_{\Pi_2}. \quad (29)$$

Zoom in further by looking only at Π_1 , we have the following relationships

$$\Pi_1 = \underbrace{r_i^{(1)T} W}_{\xi_1} - \underbrace{r_j^{(1)T} W}_{\xi_2} \quad (30)$$

$$\xi_1 = \frac{1}{\sqrt{\zeta}} r_i^{(1)T} \begin{bmatrix} \sum_i r_i^{(1)} & \sum_i r_i^{(2)} & \dots & \sum_i r_i^{(\tau)} \end{bmatrix} \quad (31)$$

$$= \frac{1}{\sqrt{\zeta}} r_i^{(1)T} \left[(r_1^{(1)} + \dots + r_{n_1}^{(1)}) \quad \dots \quad (r_1^{(\tau)} + \dots + r_{n_\tau}^{(\tau)}) \right] \quad (32)$$

$$\xi_2 = \frac{1}{\sqrt{\zeta}} r_j^{(1)T} \begin{bmatrix} \sum_i r_i^{(1)} & \sum_i r_i^{(2)} & \dots & \sum_i r_i^{(\tau)} \end{bmatrix} \quad (33)$$

$$= \frac{1}{\sqrt{\zeta}} r_j^{(1)T} \left[(r_1^{(1)} + \dots + r_{n_1}^{(1)}) \quad \dots \quad (r_1^{(\tau)} + \dots + r_{n_\tau}^{(\tau)}) \right] \quad (34)$$

By knowing that the inner product is constrained between $[0, u_{\sigma_0}]$, we know the maximum possible value for ξ_1 and the minimum possible value for ξ_2 to be

$$\xi_1 = \frac{1}{\sqrt{\zeta}} [1 + (n_1 - 1)u_{\sigma_0} \quad n_2 u_{\sigma_0} \quad n_3 u_{\sigma_0} \quad \dots \quad n_\tau u_{\sigma_0}] \quad (35)$$

$$\xi_2 = \frac{1}{\sqrt{\zeta}} [1 \quad 0 \quad 0 \quad \dots \quad 0]. \quad (36)$$

Which leads to

$$\Pi_1 = \frac{1}{\sqrt{\zeta}}(\xi_1 - \xi_2) = \frac{1}{\sqrt{\zeta}} [(n_1 - 1)u_{\sigma_0} \quad n_2 u_{\sigma_0} \quad n_3 u_{\sigma_0} \quad \dots \quad n_{\tau} u_{\sigma_0}] \quad (37)$$

Since $\Pi_2^T = \Pi_1$ we have

$$\Pi_1 \Pi_2 = \frac{1}{\zeta} [(n_1 - 1)^2 u_{\sigma_0}^2 + n_2^2 u_{\sigma_0}^2 + n_3^2 u_{\sigma_0}^2 + \dots + n_{\tau}^2 u_{\sigma_0}^2] \quad (38)$$

$$= \frac{1}{\zeta} [(n_1 - 1)^2 + n_2^2 + n_3^2 + \dots + n_{\tau}^2] u_{\sigma_0}^2 \quad (39)$$

The lower bound for just the \mathcal{W}_1 term emerges as

$$\mathcal{W}_1 \geq \sum_{\mathcal{S}^1} \Gamma_{i,j} e^{-\frac{[(n_1 - 1)^2 + n_2^2 + n_3^2 + \dots + n_{\tau}^2] u_{\sigma_0}^2}{2\zeta \sigma_1^2}}. \quad (40)$$

To further condense the notation, we define the following constant

$$\mathcal{N}_g = \frac{1}{2\zeta} [n_1^2 + n_2^2 + \dots + (n_g - 1)^2 + \dots + n_{\tau}^2]. \quad (41)$$

Therefore, the lower bound for \mathcal{W}_1 can be simplified as

$$\mathcal{W}_1 \geq \sum_{\mathcal{S}^1} \Gamma_{i,j} e^{-\frac{\mathcal{N}_1 u_{\sigma_0}^2}{\sigma_1^2}} \quad (42)$$

and the general pattern for any \mathcal{W}_g becomes

$$\mathcal{W}_g \geq \sum_{\mathcal{S}^g} \Gamma_{i,j} e^{-\frac{\mathcal{N}_g u_{\sigma_0}^2}{\sigma_1^2}}. \quad (43)$$

The lower bound for the entire set of \mathcal{S} then becomes

$$\sum_{i,j \in \mathcal{S}} \Gamma_{i,j} e^{-\frac{(r_i - r_j)^T W W^T (r_i - r_j)}{2\sigma_1^2}} = \mathcal{W}_1 + \dots + \mathcal{W}_{\tau} \geq \underbrace{\sum_{g=1}^{\tau} \sum_{\mathcal{S}^g} \Gamma_{i,j} e^{-\frac{\mathcal{N}_g u_{\sigma_0}^2}{\sigma_1^2}}}_{\text{Lower bound}}. \quad (44)$$

For sample pairs in \mathcal{S}^c . To simplify the notation, we note that

$$-\mathcal{B}_{g_1, g_2} = - \sum_{i \in \mathcal{S}^{g_1}} \sum_{j \in \mathcal{S}^{g_2}} |\Gamma_{i,j}| e^{-\frac{(r_i^{(g_1)} - r_j^{(g_2)})^T W W^T (r_i^{(g_1)} - r_j^{(g_2)})}{2\sigma_1^2}} \quad (45)$$

$$= - \sum_{i \in \mathcal{S}^{g_1}} \sum_{j \in \mathcal{S}^{g_2}} |\Gamma_{i,j}| e^{-\frac{\text{Tr}(W^T ((r_i^{(g_1)} - r_j^{(g_1)}))((r_i^{(g_1)} - r_j^{(g_2)}))^T W)}{2\sigma_1^2}} \quad (46)$$

$$= - \sum_{i \in \mathcal{S}^{g_1}} \sum_{j \in \mathcal{S}^{g_2}} |\Gamma_{i,j}| e^{-\frac{\text{Tr}(W^T A_{i,j}^{(g_1, g_2)} W)}{2\sigma_1^2}} \quad (47)$$

$$(48)$$

We now derived the lower bound for the sample pairs in \mathcal{S}^c . We start by writing out the entire summation

sequence for \mathcal{B} .

$$\begin{aligned}
 \mathcal{B} = & -\underbrace{\sum_{i \in \mathcal{S}^1} \sum_{j \in \mathcal{S}^2} |\Gamma_{i,j}| e^{-\frac{\text{Tr}(W^T A_{i,j}^{(1,2)} W)}{2\sigma_1^2}}}_{\mathcal{B}_{1,2}} - \underbrace{\dots}_{\mathcal{B}_{g_1 \neq g_2}} - \underbrace{\sum_{i \in \mathcal{S}^1} \sum_{j \in \mathcal{S}^\tau} |\Gamma_{i,j}| e^{-\frac{\text{Tr}(W^T A_{i,j}^{(1,\tau)} W)}{2\sigma_1^2}}}_{\mathcal{B}_{1,\tau}} \\
 & - \underbrace{\sum_{i \in \mathcal{S}^2} \sum_{j \in \mathcal{S}^1} |\Gamma_{i,j}| e^{-\frac{\text{Tr}(W^T A_{i,j}^{(2,1)} W)}{2\sigma_1^2}}}_{\mathcal{B}_{2,1}} - \underbrace{\dots}_{\mathcal{B}_{g_1 \neq g_2}} - \underbrace{\sum_{i \in \mathcal{S}^2} \sum_{j \in \mathcal{S}^\tau} |\Gamma_{i,j}| e^{-\frac{\text{Tr}(W^T A_{i,j}^{(2,\tau)} W)}{2\sigma_1^2}}}_{\mathcal{B}_{2,\tau}} \\
 & \dots \\
 & - \underbrace{\sum_{i \in \mathcal{S}^\tau} \sum_{j \in \mathcal{S}^1} |\Gamma_{i,j}| e^{-\frac{\text{Tr}(W^T A_{i,j}^{(\tau,1)} W)}{2\sigma_1^2}}}_{\mathcal{B}_{\tau,1}} - \underbrace{\dots}_{\mathcal{B}_{g_1 \neq g_2}} - \underbrace{\sum_{i \in \mathcal{S}^{\tau-1}} \sum_{j \in \mathcal{S}^\tau} |\Gamma_{i,j}| e^{-\frac{\text{Tr}(W^T A_{i,j}^{(\tau-1,\tau)} W)}{2\sigma_1^2}}}_{\mathcal{B}_{\tau-1,\tau}}
 \end{aligned} \tag{49}$$

Using a similar approach with the terms from \mathcal{W} , note that \mathcal{B} is a negative value, so we need to maximize this term to obtain a lower bound. Consequently, the key is to determine the **minimal** possible values for each exponent term. Since every one of them will behave very similarly, we can simply look at the numerator of the exponent from $\mathcal{B}_{1,2}$ and then arrive to a more general conclusion. Given W_s as W , our goal is to identify the **minimal** possible value for

$$\underbrace{(r_i^{(1)} - r_j^{(2)})^T}_{{\Pi_1}} \underbrace{W W^T (r_i^{(1)} - r_j^{(2)})}_{{\Pi_2}}. \tag{50}$$

Zoom in further by looking only at Π_1 , we have the following relationships

$$\Pi_1 = \underbrace{r_i^{(1)T} W}_{\xi_1} - \underbrace{r_j^{(2)T} W}_{\xi_2} \tag{51}$$

$$\xi_1 = \frac{1}{\sqrt{\zeta}} r_i^{(1)T} \left[\sum_t r_t^{(1)} \quad \sum_t r_t^{(2)} \quad \dots \quad \sum_t r_t^{(\tau)} \right] \tag{52}$$

$$= \frac{1}{\sqrt{\zeta}} r_i^{(1)T} \left[(r_1^{(1)} + \dots + r_{n_1}^{(1)}) \quad \dots \quad (r_1^{(\tau)} + \dots + r_{n_\tau}^{(\tau)}) \right] \tag{53}$$

$$\xi_2 = \frac{1}{\sqrt{\zeta}} r_j^{(2)T} \left[\sum_t r_t^{(1)} \quad \sum_t r_t^{(2)} \quad \dots \quad \sum_t r_t^{(\tau)} \right] \tag{54}$$

$$= \frac{1}{\sqrt{\zeta}} r_j^{(2)T} \left[(r_1^{(1)} + \dots + r_{n_1}^{(1)}) \quad \dots \quad (r_1^{(\tau)} + \dots + r_{n_\tau}^{(\tau)}) \right] \tag{55}$$

By knowing that the inner product is constrained between $[0, u_{\sigma_0}]$, we know the **minimum** possible value for ξ_1 and the **maximum** possible value for ξ_2 to be

$$\xi_1 = \frac{1}{\sqrt{\zeta}} [1 \quad 0 \quad 0 \quad \dots \quad 0] \tag{56}$$

$$\xi_2 = \frac{1}{\sqrt{\zeta}} [n_1 u_{\sigma_0} \quad 1 + (n_2 - 1) u_{\sigma_0} \quad n_3 u_{\sigma_0} \quad \dots \quad n_\tau u_{\sigma_0}] \tag{57}$$

Which leads to

$$\Pi_1 = \frac{1}{\sqrt{\zeta}} (\xi_1 - \xi_2) = \frac{1}{\sqrt{\zeta}} [1 - n_1 u_{\sigma_0} \quad -(1 + (n_2 - 1) u_{\sigma_0}) \quad -n_3 u_{\sigma_0} \quad \dots \quad -n_\tau u_{\sigma_0}] \tag{58}$$

Since $\Pi_2^T = \Pi_1$ we have

$$\Pi_1 \Pi_2 = \frac{1}{\zeta} [(1 - n_1 u_{\sigma_0})^2 + (1 + (n_2 - 1) u_{\sigma_0})^2 + n_3^2 u_{\sigma_0}^2 + \dots + n_\tau^2 u_{\sigma_0}^2]. \quad (59)$$

The lower bound for just the $\mathcal{B}_{1,2}$ term emerges as

$$-\mathcal{B}_{1,2} \geq - \sum_{S^1} \sum_{S^2} |\Gamma_{i,j}| e^{-\frac{(1-n_1 u_{\sigma_0})^2 + (1+(n_2-1) u_{\sigma_0})^2 + n_3^2 u_{\sigma_0}^2 + \dots + n_\tau^2 u_{\sigma_0}^2}{2\zeta \sigma_1^2}}. \quad (60)$$

To further condense the notation, we define the following function

$$\begin{aligned} \mathcal{N}_{g_1, g_2}(u_{\sigma_0}) &= \frac{1}{2\zeta} [n_1^2 u_{\sigma_0}^2 + n_2^2 u_{\sigma_0}^2 + \dots \\ &\quad + (1 - n_{g_1} u_{\sigma_0})^2 + \dots + (1 + (n_{g_2} - 1) u_{\sigma_0})^2 \\ &\quad + \dots + n_\tau^2 u_{\sigma_0}^2]. \end{aligned} \quad (61)$$

Note that while for S , the u_{σ_0} term can be separated out. But here, we cannot, and therefore \mathcal{N} here must be a function of u_{σ_0} . Therefore, the lower bound for $\mathcal{B}_{1,2}$ can be simplified into

$$-\mathcal{B}_{1,2} \geq - \sum_{S^1} \sum_{S^2} |\Gamma_{i,j}| e^{-\frac{\mathcal{N}_{1,2}(u_{\sigma_0})}{\sigma_1^2}} \quad (62)$$

and the general pattern for any \mathcal{B}_{g_1, g_2} becomes

$$-\mathcal{B}_{g_1, g_2} \geq - \sum_{S^{g_1}} \sum_{S^{g_2}} |\Gamma_{i,j}| e^{-\frac{\mathcal{N}_{g_1, g_2}(u_{\sigma_0})}{\sigma_1^2}}. \quad (63)$$

The lower bound for the entire set of S^c then becomes

$$-\sum_{i,j \in S^c} |\Gamma_{i,j}| e^{-\frac{(r_i - r_j)^T W W^T (r_i - r_j)}{2\sigma_1^2}} = -\mathcal{B}_{1,2} - \mathcal{B}_{1,3} - \dots - \mathcal{B}_{\tau-1,\tau} \quad (64)$$

$$\geq - \underbrace{\sum_{g_1 \neq g_2} \sum_{i \in S^{g_1}} \sum_{j \in S^{g_2}} |\Gamma_{i,j}| e^{-\frac{\mathcal{N}_{g_1, g_2}(u_{\sigma_0})}{\sigma_1^2}}}_{\text{Lower bound}}. \quad (65)$$

Putting S and S^c Together.

$$\mathcal{H} = \mathcal{W} + \mathcal{B} \quad (66)$$

$$\geq \underbrace{\sum_{g=1}^{\tau} \sum_{S^g} |\Gamma_{i,j}| e^{-\frac{\mathcal{N}_g u_{\sigma_0}^2}{\sigma_1^2}}}_{\text{Lower bound of } \mathcal{W}} - \underbrace{\sum_{g_1 \neq g_2} \sum_{i \in S^{g_1}} \sum_{j \in S^{g_2}} |\Gamma_{i,j}| e^{-\frac{\mathcal{N}_{g_1, g_2}(u_{\sigma_0})}{\sigma_1^2}}}_{\text{Lower bound of } \mathcal{B}}. \quad (67)$$

Therefore, we have identified a lower bound that is a function of σ_0 and σ_1 where

$$\mathcal{L}(\sigma_0, \sigma_1) = \sum_{g=1}^{\tau} \sum_{S^g} |\Gamma_{i,j}| e^{-\frac{\mathcal{N}_g u_{\sigma_0}^2}{\sigma_1^2}} - \sum_{g_1 \neq g_2} \sum_{i \in S^{g_1}} \sum_{j \in S^{g_2}} |\Gamma_{i,j}| e^{-\frac{\mathcal{N}_{g_1, g_2}(u_{\sigma_0})}{\sigma_1^2}}. \quad (68)$$

From the lower bound, it is obvious why it is a function of σ_1 . The lower bound is also a function of σ_0 because u_{σ_0} is actually a function of σ_0 . To specifically clarify this point, we have the next lemma.

□

Lemma 2. The u_{σ_0} used in Lemma 1 is a function of σ_0 where u_{σ_0} approaches to zero as σ_0 approaches to zero, i.e.

$$\lim_{\sigma_0 \rightarrow 0} u_{\sigma_0} = 0. \quad (69)$$

Assumptions and Notations.

1. We use Fig. 5 to help clarify the notations. We here only look at the last 2 layers.
2. We let \mathcal{H}_0 be the \mathcal{H} of the last layer, and \mathcal{H}_1 , the \mathcal{H} of the current layer.
3. The input of the data is X with each sample as x_i , and the output of the previous layer are denoted as r_i . ψ_{σ_0} is the feature map of the previous layer using σ_0 and ψ_{σ_1} corresponds to the current layer.

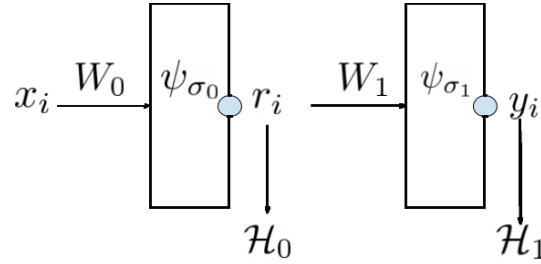


Figure 5: Figure of a 2 layer network.

4. As defined from Lemma 1, among all $r_i \neq r_j$ pairs, there exists an optimal r_i^*, r_j^* pair where $\langle r_i^*, r_j^* \rangle \geq \langle r_i, r_j \rangle$ $\forall r_i \neq r_i^*$ and $r_j \neq r_j^*$. We denote this maximum inner product as

$$u_{\sigma_0} = \langle r_i^*, r_j^* \rangle. \quad (70)$$

Proof.

Given Fig. 5, the equation for \mathcal{H}_0 is

$$\mathcal{H}_0 = \sum_{i,j \in \mathcal{S}} \Gamma_{i,j} e^{-\frac{(x_i - x_j)^T W W^T (x_i - x_j)}{2\sigma_0^2}} - \sum_{i,j \in \mathcal{S}^c} |\Gamma_{i,j}| e^{-\frac{(x_i - x_j)^T W W^T (x_i - x_j)}{2\sigma_0^2}} \quad (71)$$

$$= \sum_{i,j \in \mathcal{S}} \Gamma_{i,j} \langle \psi_{\sigma_0}(x_i), \psi_{\sigma_0}(x_j) \rangle - \sum_{i,j \in \mathcal{S}^c} |\Gamma_{i,j}| \langle \psi_{\sigma_0}(x_i), \psi_{\sigma_0}(x_j) \rangle \quad (72)$$

Notice that as $\sigma_0 \rightarrow 0$, we have

$$\lim_{\sigma_0 \rightarrow 0} \langle \psi_{\sigma_0}(x_i), \psi_{\sigma_0}(x_j) \rangle = \begin{cases} 0 & \forall i \neq j \\ 1 & \forall i = j \end{cases}. \quad (73)$$

In other words, as $\sigma_0 \rightarrow 0$, the samples r_i in the RKHS of a Gaussian kernel approaches orthogonal to all other samples. Given this fact, it also implies that the σ_0 controls the inner product magnitude in RKHS space of the maximum sample pair r_i^*, r_j^* . We define this maximum inner product as

$$\langle \psi_{\sigma_0}(x_i^*), \psi_{\sigma_0}(x_j^*) \rangle \geq \langle \psi_{\sigma_0}(x_i), \psi_{\sigma_0}(x_j) \rangle \quad (74)$$

or equivalently

$$\langle r_i^*, r_j^* \rangle \geq \langle r_i, r_j \rangle \quad (75)$$

Therefore, given a σ_0 , it controls the upper bound of the inner product. Notice that as $\sigma_0 \rightarrow 0$, every sample in RKHS becomes orthogonal. Therefore, the upper bound of $\langle r_i, r_j \rangle$ also approaches 0 when $r_i \neq r_j$. From this, we see the relationship

$$\lim_{\sigma_0 \rightarrow 0} u_{\sigma_0} = \lim_{\sigma_0 \rightarrow 0} \exp(-(|\cdot|/\sigma_0^2)) = 0 \quad (76)$$

, where $|\cdot|$ is bounded and has a minimum and maximum, because we have finite number of samples.

□

Lemma 3. Given any fixed $\sigma_1 > 0$, the lower bound $\mathcal{L}(\sigma_0, \sigma_1)$ is a function with respect to σ_0 and as $\sigma_0 \rightarrow 0$, $\mathcal{L}(\sigma_0, \sigma_1)$ approaches the function

$$\mathcal{L}(\sigma_1) = \sum_{g=1}^{\tau} \sum_{\mathcal{S}^g} \Gamma_{i,j} - \sum_{g_1 \neq g_2}^{\tau} \sum_{i \in \mathcal{S}^{g_1}} \sum_{j \in \mathcal{S}^{g_2}} |\Gamma_{i,j}| e^{-\frac{1}{\zeta \sigma_1^2}}. \quad (77)$$

At this point, if we let $\sigma_1 \rightarrow 0$, we have

$$\lim_{\sigma_1 \rightarrow 0} \mathcal{L}(\sigma_1) = \sum_{i,j \in \mathcal{S}} \Gamma_{i,j} \quad (78)$$

$$= \mathcal{H}^*. \quad (79)$$

Proof.

Given Lemma 2, we know that

$$\lim_{\sigma_0 \rightarrow 0} u_{\sigma_0} = 0. \quad (80)$$

Therefore, having $\sigma_0 \rightarrow 0$ is equivalent to having $u_{\sigma_0} \rightarrow 0$. Since Lemma 1 provide the equation of a lower bound that is a function of u_{σ_0} , this lemma is proven by simply evaluating $\mathcal{L}(\sigma_0, \sigma_1)$ as $u_{\sigma_0} \rightarrow 0$. Following these steps, we have

$$\mathcal{L}(\sigma_1) = \lim_{u_{\sigma_0} \rightarrow 0} \sum_{g=1}^{\tau} \sum_{\mathcal{S}^g} \Gamma_{i,j} e^{-\frac{\mathcal{N}_g u_{\sigma_0}^2}{\sigma_1^2}} - \sum_{g_1 \neq g_2}^{\tau} \sum_{i \in \mathcal{S}^{g_1}} \sum_{j \in \mathcal{S}^{g_2}} |\Gamma_{i,j}| e^{-\frac{\mathcal{N}_{g_1, g_2}(u_{\sigma_0})}{\sigma_1^2}}, \quad (81)$$

$$= \sum_{g=1}^{\tau} \sum_{\mathcal{S}^g} \Gamma_{i,j} - \sum_{g_1 \neq g_2}^{\tau} \sum_{i \in \mathcal{S}^{g_1}} \sum_{j \in \mathcal{S}^{g_2}} |\Gamma_{i,j}| e^{-\frac{1}{\zeta \sigma_1^2}}. \quad (82)$$

At this point, as $\sigma_1 \rightarrow 0$, our lower bound reaches the global maximum

$$\lim_{\sigma_1 \rightarrow 0} \mathcal{L}(\sigma_1) = \sum_{g=1}^{\tau} \sum_{\mathcal{S}^g} \Gamma_{i,j} = \sum_{i,j \in \mathcal{S}} \Gamma_{i,j} \quad (83)$$

$$= \mathcal{H}^*. \quad (84)$$

□

Lemma 4. Given any \mathcal{H}_{l-2} , $\delta > 0$, there exists a $\sigma_0 > 0$ and $\sigma_1 > 0$ such that

$$\mathcal{H}^* - \mathcal{H}_l \leq \delta. \quad (85)$$

Proof.

Observation 1.

Note that the objective of \mathcal{H}_l is

$$\begin{aligned} \mathcal{H}_l = \max_W \sum_{i,j \in \mathcal{S}} \Gamma_{i,j} e^{-\frac{(r_i^{(\mathcal{S})} - r_j^{(\mathcal{S})})^T W W^T (r_i^{(\mathcal{S})} - r_j^{(\mathcal{S})})}{2\sigma_1^2}} \\ - \sum_{i,j \in \mathcal{S}^c} |\Gamma_{i,j}| e^{-\frac{(r_i^{(\mathcal{S}^c)} - r_j^{(\mathcal{S}^c)})^T W W^T (r_i^{(\mathcal{S}^c)} - r_j^{(\mathcal{S}^c)})}{2\sigma_1^2}}. \end{aligned} \quad (86)$$

Since the Gaussian kernel is bounded between 0 and 1, the theoretical maximum of \mathcal{H}^* is when the kernel is 1 for \mathcal{S} and 0 for \mathcal{S}^c with the theoretical maximum as $\mathcal{H}^* = \sum_{i,j \in \mathcal{S}} \Gamma_{i,j}$. Therefore Eq. (85) inequality is equivalent to

$$\sum_{i,j \in \mathcal{S}} \Gamma_{i,j} - \mathcal{H}_l \leq \delta. \quad (87)$$

Observation 2.

If we choose a σ_0 such that

$$\mathcal{L}^*(\sigma_1) - \mathcal{L}(\sigma_0, \sigma_1) \leq \frac{\delta}{2} \quad \text{and} \quad \mathcal{H}^* - \mathcal{L}^*(\sigma_1) \leq \frac{\delta}{2} \quad (88)$$

then we have identified the condition where $\sigma_0 > 0$ and $\sigma_1 > 0$ such that

$$\sum_{i,j \in \mathcal{S}} \Gamma_{i,j} - \mathcal{L}(\sigma_0, \sigma_1) \leq \delta. \quad (89)$$

Note that the $\mathcal{L}^*(\sigma_1)$ is a continuous function of σ_1 . Therefore, a σ_1 exists such that $\mathcal{L}^*(\sigma_1)$ can be set arbitrary close to \mathcal{H}^* . Hence, we choose an σ_1 that has the following property:

$$\mathcal{H}^* - \mathcal{L}^*(\sigma_1) \leq \frac{\delta}{2}. \quad (90)$$

We next fix σ_1 , we also know $\mathcal{L}(\sigma_0, \sigma_1)$ is a continuous function of σ_0 , and it has a limit $\mathcal{L}^*(\sigma_1)$ as σ_0 approaches to 0, hence there exists a σ_0 , where

$$\mathcal{L}^*(\sigma_1) - \mathcal{L}(\sigma_0, \sigma_1) \leq \frac{\delta}{2} \quad (91)$$

Then we have:

$$\mathcal{L}^*(\sigma_1) - \mathcal{L}(\sigma_0, \sigma_1) \leq \frac{\delta}{2} \quad \text{and} \quad \mathcal{H}^* - \mathcal{L}^*(\sigma_1) \leq \frac{\delta}{2}. \quad (92)$$

By adding the two $\frac{\delta}{2}$, we conclude the proof. \square

Lemma 5. *There exists a Kernel Sequence $\{\phi_l\}_{l=1}^L$ parameterized by a set of weights W_l and a set of bandwidths σ_l such that*

$$\lim_{l \rightarrow \infty} \mathcal{H}_l = \mathcal{H}^*, \quad \mathcal{H}_{l+1} > \mathcal{H}_l \quad \forall l \quad (93)$$

Before, the proof, we use the following figure, Fig. 6, to illustrate the relationship between *Kernel Sequence* $\{\phi_l\}_{l=1}^L$ that generates the *H-Sequence* $\{\mathcal{H}_l\}_{l=1}^L$. By solving a network greedily, we separate the network into L separable problems. At each additional layer, we rely on the weights learned from the previous layer. At each network, we find σ_{l-1} , σ_l , and W_l for the next network. We also note that since we only need to prove the existence of a solution, this proof is done by **Proof by Construction**, i.e, we only need to show an example of its existence. Therefore, this proof consists of us constructing a *H-Sequence* which satisfies the lemma.

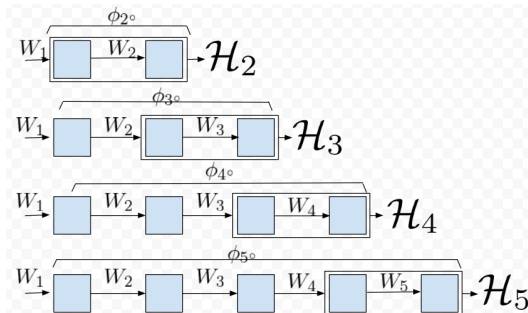


Figure 6: Relating *Kernel Sequence* to *H-Sequence*.

Proof.

We first note that from Lemma 4, we have previously proven given any \mathcal{H}_{l-2} , $\delta > 0$, there exists a $\sigma_0 > 0$ and $\sigma_1 > 0$ such that

$$\mathcal{H}^* - \mathcal{H}_l \leq \delta_l. \quad (94)$$

This implies that based on Fig. 6, at any given layer, we could reach arbitrarily close to \mathcal{H}^* . Given this, we list the 2 steps to build the \mathcal{H} -Sequence.

Step 1: Define $\{\mathcal{E}_n\}_{n=1}^\infty$ as a sequence of numbers $\mathcal{H}^* - \frac{\mathcal{H}^* - \mathcal{H}_0}{n}$ on the real line. We have the following properties for this sequence:

$$\lim_{n \rightarrow \infty} \mathcal{E}_n = \mathcal{H}^*, \quad \mathcal{E}_1 = \mathcal{H}_0. \quad (95)$$

Using these two properties, for any $\mathcal{H}_{l-1} \in [\mathcal{H}_0, \mathcal{H}^*]$ there exist an unique n , where

$$\mathcal{E}_n \leq \mathcal{H}_{l-1} < \mathcal{E}_{n+1}. \quad (96)$$

Step 2: For any given l , we choose δ_l to satisfies Eq. (94) by the following procedure, First find an n that satisfies

$$\mathcal{E}_n \leq \mathcal{H}_{l-1} < \mathcal{E}_{n+1}, \quad (97)$$

and second define δ_l to be

$$\delta_l = \mathcal{H}^* - \mathcal{E}_{n+1}. \quad (98)$$

To satisfy Eq. (94), the following must be true.

$$\mathcal{H}^* - \mathcal{H}_{l-1} \leq \delta_{l-1}. \quad (99)$$

and further we found n such that

$$\mathcal{E}_n \leq \mathcal{H}_{l-1} < \mathcal{E}_{n+1} \implies \mathcal{H}^* - \mathcal{E}_n \geq \mathcal{H}^* - \mathcal{H}_{l-1} > \mathcal{H}^* - \mathcal{E}_{n+1}. \quad (100)$$

Thus combining Eq. (98), Eq. (99), and Eq. (100) we have

$$\delta_{l-1} > \delta_l. \quad (101)$$

Therefore, $\{\delta_l\}$ is a decreasing sequence.

Step 3: Note that $\{\mathcal{E}_n\}$ is a converging sequence where

$$\lim_{n \rightarrow \infty} \mathcal{H}^* - \frac{\mathcal{H}^* - \mathcal{H}_0}{n} = \mathcal{H}^*. \quad (102)$$

Therefore, $\{\Delta_n\} = \mathcal{H}^* - \{\mathcal{E}_n\}$ is also a converging sequence where

$$\lim_{n \rightarrow \infty} \mathcal{H}^* - \mathcal{H}^* + \frac{\mathcal{H}^* - \mathcal{H}_0}{n} = 0 \quad (103)$$

and $\{\delta_l\}$ is a subsequence of $\{\Delta_l\}$. Since any subsequence of a converging sequence also converges to the same limit, we know that

$$\lim_{l \rightarrow \infty} \delta_l = 0. \quad (104)$$

Following this construction, if we always choose \mathcal{H}_l such that

$$\mathcal{H}^* - \mathcal{H}_l \leq \delta_l. \quad (105)$$

As $l \rightarrow \infty$, the inequality becomes

$$\mathcal{H}^* - \lim_{l \rightarrow \infty} \mathcal{H}_l \leq \lim_{l \rightarrow \infty} \delta_l, \quad (106)$$

$$\leq 0. \quad (107)$$

Since we know that

$$\mathcal{H}^* - \mathcal{H}_l \geq 0 \forall l. \quad (108)$$

The condition of

$$0 \leq \mathcal{H}^* - \lim_{l \rightarrow \infty} \mathcal{H}_l \leq 0 \quad (109)$$

is true only if

$$\mathcal{H}^* - \lim_{l \rightarrow \infty} \mathcal{H}_l = 0. \quad (110)$$

This allows us to conclude

$$\mathcal{H}^* = \lim_{l \rightarrow \infty} \mathcal{H}_l. \quad (111)$$

Proof of the Monotonic Improvement.

Given Eq. (96) and Eq. (98), at each step we have the following:

$$\mathcal{H}_{l-1} < \mathcal{E}_{n+1} \quad (112)$$

$$\leq \mathcal{H}^* - \delta_l. \quad (113)$$

Rearranging this inequality, we have

$$\delta_l < \mathcal{H}^* - \mathcal{H}_{l-1}. \quad (114)$$

By combining the inequalities from Eq. (114) and Eq. (105), we have the following relationships.

$$\mathcal{H}^* - \mathcal{H}_l \leq \delta_l < \mathcal{H}^* - \mathcal{H}_{l-1} \quad (115)$$

$$\mathcal{H}^* - \mathcal{H}_l < \mathcal{H}^* - \mathcal{H}_{l-1} \quad (116)$$

$$-\mathcal{H}_l < -\mathcal{H}_{l-1} \quad (117)$$

$$\mathcal{H}_l > \mathcal{H}_{l-1}, \quad (118)$$

$$(119)$$

which concludes the proof of theorem. \square

Appendix B Proof for Theorem 3

Theorem 3. Given \mathcal{H}_l as the empirical risk at layer $l \neq L$, we have

$$\frac{\partial}{\partial W_l} \mathcal{H}_l(W_s) \neq 0 \quad (120)$$

Proof. Given $\frac{1}{\sqrt{\zeta}}$ as a normalizing constant for $W_s = \frac{1}{\sqrt{\zeta}} \sum_{\alpha} r_{\alpha}$ such that $W^T W = I$. We start with the Lagrangian

$$\mathcal{L} = - \sum_{i,j} \Gamma_{i,j} e^{-\frac{(r_i - r_j)^T W W^T (r_i - r_j)}{2\sigma^2}} - \text{Tr}(\Lambda(W^T W - I)). \quad (121)$$

If we now take the derivative with respect to the Lagrange, we get

$$\nabla \mathcal{L} = \frac{1}{\sigma^2} \sum_{i,j} \Gamma_{i,j} e^{-\frac{(r_i - r_j)^T W W^T (r_i - r_j)}{2\sigma^2}} (r_i - r_j)(r_i - r_j)^T W - 2W\Lambda. \quad (122)$$

By setting the gradient to 0, we have

$$\left[\frac{1}{2\sigma^2} \sum_{i,j} \Gamma_{i,j} e^{-\frac{(r_i - r_j)^T W W^T (r_i - r_j)}{2\sigma^2}} (r_i - r_j)(r_i - r_j)^T \right] W = W\Lambda. \quad (123)$$

$$Q_l W = W\Lambda. \quad (124)$$

From Eq. (124), we see that W is only the optimal solution when W is the eigenvector of Q_l . Therefore, by setting W to $W_s = \frac{1}{\sqrt{\zeta}} \sum_{\alpha} r_{\alpha}$, it is not guaranteed to yield an optimal for all σ_l . \square

Appendix C Proof for Theorem 2

Theorem 2: As $l \rightarrow \infty$ and $\mathcal{H}_l \rightarrow \mathcal{H}^*$, the following properties are satisfied:

I the scatter ratio approaches 0 where

$$\lim_{l \rightarrow \infty} \frac{\text{Tr}(S_w^l)}{\text{Tr}(S_b^l)} = 0 \quad (125)$$

II the Kernel Sequence converges to the following kernel:

$$\lim_{l \rightarrow \infty} \mathcal{K}(x_i, x_j)^l = \mathcal{K}^* = \begin{cases} 0 & \forall i, j \in \mathcal{S}^c \\ 1 & \forall i, j \in \mathcal{S} \end{cases}. \quad (126)$$

Proof. We start by proving condition II starting from the \mathcal{H} objective using a GK

$$\max_W \sum_{i,j \in \mathcal{S}} \Gamma_{i,j} \mathcal{K}_W(r_i, r_j) - \sum_{i,j \in \mathcal{S}^c} |\Gamma_{i,j}| \mathcal{K}_W(r_i, r_j) \quad (127)$$

$$\max_W \sum_{i,j \in \mathcal{S}} \Gamma_{i,j} e^{-\frac{(r_i - r_j)^T W W^T (r_i - r_j)}{2\sigma^2}} - \sum_{i,j \in \mathcal{S}^c} |\Gamma_{i,j}| e^{-\frac{(r_i - r_j)^T W W^T (r_i - r_j)}{2\sigma^2}} \quad (128)$$

Given that $\mathcal{H}_l \rightarrow \mathcal{H}^*$, and the fact that $0 \leq \mathcal{K}_W \leq 1$, this implies that the following condition must be true:

$$\mathcal{H}^* = \sum_{i,j \in \mathcal{S}} \Gamma_{i,j} = \sum_{i,j \in \mathcal{S}} \Gamma_{i,j}(1) - \sum_{i,j \in \mathcal{S}^c} |\Gamma_{i,j}|(0). \quad (129)$$

Based on Eq. (94), our construction at each layer ensures to satisfy

$$\mathcal{H}^* - \mathcal{H}_l \leq \delta_l. \quad (130)$$

Substituting the definition of \mathcal{H}^* and \mathcal{H}_l , we have

$$\sum_{i,j \in \mathcal{S}} \Gamma_{i,j}(1) - \left[\sum_{i,j \in \mathcal{S}} \Gamma_{i,j} \mathcal{K}_W(r_i, r_j) - \sum_{i,j \in \mathcal{S}^c} |\Gamma_{i,j}| \mathcal{K}_W(r_i, r_j) \right] \leq \delta_l \quad (131)$$

$$\sum_{i,j \in \mathcal{S}} \Gamma_{i,j}(1 - \mathcal{K}_W(r_i, r_j)) + \sum_{i,j \in \mathcal{S}^c} |\Gamma_{i,j}| \mathcal{K}_W(r_i, r_j) \leq \delta_l. \quad (132)$$

Since every term within the summation in Eq. (132) is positive, this implies

$$1 - \mathcal{K}_W(r_i, r_j) \leq \delta_l \quad i, j \in \mathcal{S} \quad (133)$$

$$\mathcal{K}_W(r_i, r_j) \leq \delta_l \quad i, j \in \mathcal{S}^c. \quad (134)$$

So as $l \rightarrow \infty$ and $\delta_l \rightarrow 0$, every component getting closer to limit Kernel, i.e, taking the limit from both sides and using the fact that is proven is theorem 1 $\lim_{l \rightarrow \infty} \delta_l = 0$ leads to

$$\lim_{l \rightarrow \infty} 1 \leq \mathcal{K}_W(r_i, r_j) \quad i, j \in \mathcal{S} \quad (135)$$

$$\lim_{l \rightarrow \infty} \mathcal{K}_W(r_i, r_j) \leq 0 \quad i, j \in \mathcal{S}^c \quad (136)$$

both terms must instead be strictly equality. Therefore, we see that at the limit point \mathcal{K}_W would have the form

$$\mathcal{K}^* = \begin{cases} 0 & \forall i, j \in \mathcal{S}^c \\ 1 & \forall i, j \in \mathcal{S} \end{cases}. \quad (137)$$

First Property:

Using Eq. (133) and Eq. (134) we have:

$$1 - \delta_l \leq e^{-\frac{(r_i - r_j)^T W W^T (r_i - r_j)}{2\sigma^2}} \quad i, j \in \mathcal{S} \quad (138)$$

$$e^{-\frac{(r_i - r_j)^T W W^T (r_i - r_j)}{2\sigma^2}} \leq \delta_l \quad i, j \in \mathcal{S}^c. \quad (139)$$

As $\lim_{l \rightarrow \infty} \delta_l = 0$, taking the limit from both side leads to:

$$\begin{cases} e^{-\frac{(r_i - r_j)^T W W^T (r_i - r_j)}{2\sigma^2}} = 1 & \forall i, j \in \mathcal{S} \\ e^{-\frac{(r_i - r_j)^T W W^T (r_i - r_j)}{2\sigma^2}} = 0 & \forall i, j \in \mathcal{S}^c \end{cases}. \quad (140)$$

If we take the log of the conditions, we get

$$\begin{cases} \frac{1}{2\sigma^2} (r_i - r_j)^T W W^T (r_i - r_j) = 0 & \forall i, j \in \mathcal{S} \\ \frac{1}{2\sigma^2} (r_i - r_j)^T W W^T (r_i - r_j) = \infty & \forall i, j \in \mathcal{S}^c \end{cases}. \quad (141)$$

This implies that as $l \rightarrow \infty$ we have

$$\lim_{l \rightarrow \infty} \sum_{i, j \in \mathcal{S}} \frac{1}{2\sigma^2} (r_i - r_j)^T W W^T (r_i - r_j) = \lim_{l \rightarrow \infty} \text{Tr}(S_w) = 0. \quad (142)$$

$$\lim_{l \rightarrow \infty} \sum_{i, j \in \mathcal{S}^c} \frac{1}{2\sigma^2} (r_i - r_j)^T W W^T (r_i - r_j) = \lim_{l \rightarrow \infty} \text{Tr}(S_b) = \infty, \quad (143)$$

This yields the ratio

$$\lim_{\mathcal{H}_l \rightarrow \mathcal{H}^*} \frac{\text{Tr}(S_w)}{\text{Tr}(S_b)} = \frac{0}{\infty} = 0. \quad (144)$$

□

Appendix D Proof for Theorem 4

Theorem 4: Eq. (4) objective is equivalent to

$$\sum_{i, j} \Gamma_{i, j} e^{-\frac{(r_i - r_j)^T W W^T (r_i - r_j)}{2\sigma^2}} (r_i^T W W^T r_j) - \sum_i D_i(W) \|W^T r_i\|_2. \quad (145)$$

Proof. Let $A_{i, j} = (r_i - r_j)(r_i - r_j)^T$. Given the Lagranian of the HSIC objective as

$$\mathcal{L} = - \sum_{i, j} \Gamma_{i, j} e^{-\frac{(r_i - r_j)^T W W^T (r_i - r_j)}{2\sigma^2}} - \text{Tr}[\Lambda(W^T W - I)]. \quad (146)$$

Our layer wise HSIC objective becomes

$$\min_W - \sum_{i, j} \Gamma_{i, j} e^{-\frac{(r_i - r_j)^T W W^T (r_i - r_j)}{2\sigma^2}} - \text{Tr}[\Lambda(W^T W - I)]. \quad (147)$$

We take the derivative of the Lagrangian, the expression becomes

$$\nabla_W \mathcal{L}(W, \Lambda) = \sum_{i, j} \frac{\Gamma_{i, j}}{\sigma^2} e^{-\frac{\text{Tr}(W^T A_{i, j} W)}{2\sigma^2}} A_{i, j} W - 2W\Lambda. \quad (148)$$

Setting the gradient to 0, and consolidate some scalar values into $\hat{\Gamma}_{i,j}$, we get the expression

$$\left[\sum_{i,j} \frac{\Gamma_{i,j}}{2\sigma^2} e^{-\frac{\text{Tr}(W^T A_{i,j} W)}{2\sigma^2}} A_{i,j} \right] W = W\Lambda \quad (149)$$

$$\left[\frac{1}{2} \sum_{i,j} \hat{\Gamma}_{i,j} A_{i,j} \right] W = W\Lambda \quad (150)$$

$$QW = W\Lambda. \quad (151)$$

From here, we see that the optimal solution is an eigenvector of Q . Based on ISM, it further proved that the optimal solution is not just any eigenvector, but the eigenvectors associated with the smallest values of Q . From this logic, ISM solves objective (147) with a surrogate objective

$$\min_W \quad \text{Tr} \left(W^T \left[\frac{1}{2} \sum_{i,j} \hat{\Gamma}_{i,j} A_{i,j} \right] W \right) \quad \text{s.t. } W^T W = I. \quad (152)$$

Given $D_{\hat{\Gamma}}$ as the degree matrix of $\hat{\Gamma}$ and $R = [r_1, r_2, \dots]^T$, ISM further shows that Eq. (152) can be written into

$$\min_W \quad \text{Tr} \left(W^T R^T \left[D_{\hat{\Gamma}} - \hat{\Gamma} \right] RW \right) \quad \text{s.t. } W^T W = I \quad (153)$$

$$\max_W \quad \text{Tr} \left(W^T R^T \left[\hat{\Gamma} - D_{\hat{\Gamma}} \right] RW \right) \quad \text{s.t. } W^T W = I \quad (154)$$

$$\max_W \quad \text{Tr} \left(W^T R^T \hat{\Gamma} RW \right) - \text{Tr} \left(W^T R^T D_{\hat{\Gamma}} RW \right) \quad \text{s.t. } W^T W = I \quad (155)$$

$$\max_W \quad \text{Tr} \left(\hat{\Gamma} RWW^T R^T \right) - \text{Tr} \left(D_{\hat{\Gamma}} RWW^T R^T \right) \quad \text{s.t. } W^T W = I \quad (156)$$

$$\max_W \quad \sum_{i,j} \hat{\Gamma}_{i,j} [RWW^T R^T]_{i,j} - \sum_{i,j} D_{\hat{\Gamma}}_{i,j} [RWW^T R^T]_{i,j} \quad \text{s.t. } W^T W = I. \quad (157)$$

Since the jump from Eq. (152) can be intimidating for those not familiar with the literature, we included a more detailed derivation in App. E.

Note that the degree matrix $D_{\hat{\Gamma}}$ only have non-zero diagonal elements, all of its off diagonal are 0. Given $[RWW^T R^T]_{i,j} = (r_i^T W W^T r_j)$, the objective becomes

$$\max_W \quad \sum_{i,j} \hat{\Gamma}_{i,j} (r_i^T W W^T r_j) - \sum_i D_i(W) \|W^T r_i\|_2 \quad \text{s.t. } W^T W = I. \quad (158)$$

Here, we treat D_i as a penalty weight on the norm of the $W^T r_i$ for every sample. \square

To better understand the behavior of $D_i(W)$, note that $\hat{\Gamma}$ matrix looks like

$$\hat{\Gamma} = \frac{1}{\sigma^2} \begin{bmatrix} \left[\Gamma_S e^{-\frac{(r_i - r_j)^T W W^T (r_i - r_j)}{2\sigma^2}} \right] & \left[-|\Gamma_{S^c}| e^{-\frac{(r_i - r_j)^T W W^T (r_i - r_j)}{2\sigma^2}} \right] & \dots \\ \left[-|\Gamma_{S^c}| e^{-\frac{(r_i - r_j)^T W W^T (r_i - r_j)}{2\sigma^2}} \right] & \left[\Gamma_{S^c} e^{-\frac{(r_i - r_j)^T W W^T (r_i - r_j)}{2\sigma^2}} \right] & \dots \\ \dots & \dots & \dots \end{bmatrix}. \quad (159)$$

The diagonal block matrix all $\Gamma_{i,j}$ elements that belong to S and the off diagonal are elements that belongs to S^c . Each penalty term is the summation of its corresponding row. Hence, we can write out the penalty term as

$$D_i(W_l) = \frac{1}{\sigma^2} \sum_{j \in S \setminus i} \Gamma_{i,j} \mathcal{K}_{W_l}(r_i, r_j) - \frac{1}{\sigma^2} \sum_{j \in S^c \setminus i} |\Gamma_{i,j}| \mathcal{K}_{W_l}(r_i, r_j). \quad (160)$$

From this, it shows that as W improve the objective, the penalty term is also increased. In fact, at its extreme as $\mathcal{H}_l \rightarrow \mathcal{H}^*$, all the negative terms are gone and all of its positive terms are maximized and this matrix approaches

$$\hat{\Gamma}^* = \frac{1}{\sigma^2} \begin{bmatrix} [\Gamma_S] & [0] & \dots \\ [0] & [\Gamma_{S^c}] & \dots \\ \dots & \dots & \dots \end{bmatrix}. \quad (161)$$

From the matrix $\hat{\Gamma}^*$ and the definition of $D_i(W_l)$, we see that as \mathcal{K}_W from \mathcal{S} increase, Since $D_i(W)$ is the degree matrix of $\hat{\Gamma}$, we see that as $\mathcal{H}_l \rightarrow \mathcal{H}^*$, we have

$$D_i^*(W) > D_i(W). \quad (162)$$

Appendix E Derivation for $\sum_{i,j} \Psi_{i,j}(x_i - x_j)(x_i - x_j)^T = 2X^T(D_\Psi - \Psi)X$

Since Ψ is a symmetric matrix, and $A_{i,j} = (x_i - x_j)(x_i - x_j)^T$, we can rewrite the expression into

$$\begin{aligned} \sum_{i,j} \Psi_{i,j} A_{i,j} &= \sum_{i,j} \Psi_{i,j} (x_i - x_j)(x_i - x_j)^T \\ &= \sum_{i,j} \Psi_{i,j} (x_i x_i^T - x_j x_i^T - x_i x_j^T + x_j x_j^T) \\ &= 2 \sum_{i,j} \Psi_{i,j} (x_i x_i^T - x_j x_i^T) \\ &= \left[2 \sum_{i,j} \Psi_{i,j} (x_i x_i^T) \right] - \left[2 \sum_{i,j} \Psi_{i,j} (x_i x_j^T) \right]. \end{aligned}$$

If we expand the 1st term, we get

$$2 \sum_i^n \sum_j^n \Psi_{i,j} (x_i x_i^T) = 2 \sum_i^n \Psi_{i,1} (x_i x_i^T) + \dots + \Psi_{i,n} (x_i x_i^T) \quad (163)$$

$$= 2 \sum_i^n [\Psi_{1,1} + \Psi_{1,2} + \dots] x_i x_i^T \quad (164)$$

$$= 2 \sum_i^n d_i x_i x_i^T \quad (165)$$

$$= 2X^T D_\Psi X \quad (166)$$

Given Ψ_i as the i th row, next we look at the 2nd term

$$2 \sum_i^n \sum_j^n \Psi_{i,j} x_i x_j^T = 2 \sum_i^n \Psi_{i,1} x_i x_1^T + \Psi_{i,2} x_i x_2^T + \Psi_{i,3} x_i x_3^T + \dots \quad (167)$$

$$= 2 \sum_i^n x_i (\Psi_{i,1} x_1^T) + x_i (\Psi_{i,2} x_2^T) + x_i (\Psi_{i,3} x_3^T) + \dots \quad (168)$$

$$= 2 \sum_i^n x_i [(\Psi_{i,1} x_1^T) + (\Psi_{i,2} x_2^T) + (\Psi_{i,3} x_3^T) + \dots] \quad (169)$$

$$= 2 \sum_i^n x_i [X^T \Psi_i^T]^T \quad (170)$$

$$= 2 \sum_i^n x_i [\Psi_i X] \quad (171)$$

$$= 2 [x_1 \Psi_1 X + x_2 \Psi_2 X + x_3 \Psi_3 X + \dots] \quad (172)$$

$$= 2 [x_1 \Psi_1 + x_2 \Psi_2 + x_3 \Psi_3 + \dots] X \quad (173)$$

$$= 2X^T \Psi X \quad (174)$$

$$(175)$$

Putting both terms together, we get

$$\sum_{i,j} \Psi_{i,j} A_{i,j} = 2X^T D_\Psi X - 2X^T \Psi X a \quad (176)$$

$$= 2X^T [D_\Psi - \Psi] X \quad (177)$$

$$(178)$$

Appendix F Proof for Corollary 1 and 2

Corollary 1: Given $\mathcal{H}_l \rightarrow \mathcal{H}^*$, the network output in IDS solves MSE via a translation of labels.

Proof.

As $\mathcal{H}_l \rightarrow \mathcal{H}^*$, Thm. 2 shows that sample of the same class are mapped into the same point. Assuming that ϕ has mapped the sample into c points $\alpha = [\alpha_1, \dots, \alpha_c]$ that's different from the truth label $\xi = [\xi_1, \dots, \xi_c]$. Then the MSE objective is minimized by translating the ϕ output by

$$\xi - \alpha. \quad (179)$$

□

Corollary 2: Given $\mathcal{H}_l \rightarrow \mathcal{H}^*$, the network output in RKHS solves CE via a change of bases.

Assumptions, and Notations.

1. n is the number of samples.
2. τ is the number of classes.
3. $y_i \in \mathbb{R}^\tau$ is the ground truth label for the i^{th} sample. It is one-hot encoded where only the j^{th} element is 1 if x_i belongs to the j^{th} class, all other elements would be 0.
4. We denote ϕ as the network, and $\hat{y}_i \in \mathbb{R}^\tau$ as the network output where $\hat{y}_i = \phi(x_i)$. We also assume that \hat{y}_i is constrained on a probability simplex where $1 = \hat{y}_i^T \mathbf{1}_n$.
5. We denote the j^{th} element of y_i , and \hat{y}_i as $y_{i,j}$ and $\hat{y}_{i,j}$ respectively.
6. We define

Orthogonality Condition: A set of samples $\{\hat{y}_1, \dots, \hat{y}_n\}$ satisfies the orthogonality condition if

$$\begin{cases} \langle \hat{y}_i, \hat{y}_j \rangle = 1 & \forall i, j \text{ same class} \\ \langle \hat{y}_i, \hat{y}_j \rangle = 0 & \forall i, j \text{ not in the same class} \end{cases}. \quad (180)$$

7. We define the Cross-Entropy objective as

$$\arg \min_{\phi} - \sum_{i=1}^n \sum_{j=1}^{\tau} y_{i,j} \log(\phi(x_i)_{i,j}). \quad (181)$$

Proof.

From Thm. 2, we know that the network ϕ output, $\{\hat{y}_1, \hat{y}_2, \dots, \hat{y}_n\}$, satisfy the orthogonality condition at \mathcal{H}^* . Then there exists a set of orthogonal bases represented by $\Xi = [\xi_1, \xi_2, \dots, \xi_c]$ that maps $\{\hat{y}_1, \hat{y}_2, \dots, \hat{y}_n\}$ to simulate the output of a softmax layer. Let $\xi_i = \hat{y}_j, j \in \mathcal{S}^i$, i.e., for the i^{th} class we arbitrary choose one of the samples from this class and assigns ξ_i of that class to be equal to the sample's output. Realize in our problem we have $\langle \hat{y}_i, \hat{y}_i \rangle = 1$, so if $\langle \hat{y}_i, \hat{y}_j \rangle = 1$, then subtracting these two would lead to $\langle \hat{y}_i, \hat{y}_i - \hat{y}_j \rangle = 0$, which is the same as $\hat{y}_i = \hat{y}_j$. So this representation is well-defined and its independent of choices of the sample from each group if they satisfy orthogonality condition. Now we define transformed labels, Y as:

$$Y = \hat{Y} \Xi. \quad (182)$$

Note that $Y = [y_1, y_2, \dots, y_n]^T$ which each y_i is a one hot vector representing the class membership of i sample in c classes. Since given Ξ as the change of basis, we can match \hat{Y} to Y exactly, CE is minimized.

□

Appendix G Dataset Details

No samples were excluded from any of the dataset.

Wine. This dataset has 13 features, 178 samples, and 3 classes. The features are continuous and heavily unbalanced in magnitude. The dataset can be downloaded at <https://archive.ics.uci.edu/ml/datasets/wine>.

Divorce. This dataset has 54 features, 170 samples, and 2 classes. The features are discrete and balanced in magnitude. The dataset can be downloaded at <https://archive.ics.uci.edu/ml/datasets/Divorce+Predictors+data+set>.

Car. This dataset has 6 features, 1728 samples and 2 classes. The features are discrete and balanced in magnitude. The dataset can be downloaded at <https://archive.ics.uci.edu/ml/datasets/Car+Evaluation>.

Cancer. This dataset has 9 features, 683 samples, and 2 classes. The features are discrete and unbalanced in magnitude. The dataset can be downloaded at [https://archive.ics.uci.edu/ml/datasets/Breast+Cancer+Wisconsin+\(Diagnostic\)](https://archive.ics.uci.edu/ml/datasets/Breast+Cancer+Wisconsin+(Diagnostic)).

Face. This dataset consists of images of 20 people in various poses. The 624 images are vectorized into 960 features. The dataset can be downloaded at <https://archive.ics.uci.edu/ml/datasets/CMU+Face+Images>.

Random. This dataset has 2 features, 80 samples and 2 classes. It is generated with a gaussian distribution where half of the samples are randomly labeled as 1 or 0.

Adversarial. This dataset has 2 features, 80 samples and 2 classes. It is generated with the following code:

```
#!/usr/bin/env python

n = 40
X1 = np.random.rand(n,2)
X2 = X1 + 0.01*np.random.randn(n,2)

X = np.vstack((X1,X2))
Y = np.vstack((np.zeros((n,1)), np.ones((n,1)) ))
```

Appendix H W_l Dimensions for each 10 Fold of each Dataset

We report the input and output dimensions of each W_l for every layer of each dataset in the form of (α, β) ; the corresponding dimension becomes $W_l \in \mathbb{R}^{\alpha \times \beta}$. Since each dataset consists of 10-folds, the network structure for each fold is reported. We note that the input of the 1st layer is the dimension of the original data. However, after the first layer, the width of the RFF becomes the output of each layer; here we use 300.

The β value is chosen during the ISM algorithm. By keeping only the most dominant eigenvector of the Φ matrix, the output dimension of each layer corresponds with the rank of Φ . It can be seen from each dataset that the first layer significantly expands the rank. The expansion is generally followed by a compression of fewer and fewer eigenvalues. These results conform with the observations made by Montavon et al. [24] and Ansuini et al. [57].

Data	Layer 1	Layer 2	Layer 3	Layer 4
adversarial 1	(2, 2)	(300, 61)	(300, 35)	
adversarial 2	(2, 2)	(300, 61)	(300, 35)	
adversarial 3	(2, 2)	(300, 61)	(300, 8)	(300, 4)
adversarial 4	(2, 2)	(300, 61)	(300, 29)	
adversarial 5	(2, 2)	(300, 61)	(300, 29)	
adversarial 6	(2, 2)	(300, 61)	(300, 7)	(300, 4)
adversarial 7	(2, 2)	(300, 61)	(300, 34)	
adversarial 8	(2, 2)	(300, 12)	(300, 61)	(300, 30)
adversarial 9	(2, 2)	(300, 61)	(300, 33)	
adversarial 10	(2, 2)	(300, 61)	(300, 33)	

Data	Layer 1	Layer 2	Layer 3
Random 1	(3, 3)	(300, 47)	(300, 25)
Random 2	(3, 3)	(300, 46)	(300, 25)
Random 3	(3, 3)	(300, 46)	(300, 25)
Random 4	(3, 3)	(300, 47)	(300, 4)
Random 5	(3, 3)	(300, 47)	(300, 25)
Random 6	(3, 3)	(300, 45)	(300, 23)
Random 7	(3, 3)	(300, 45)	(300, 25)
Random 8	(3, 3)	(300, 45)	(300, 21)
Random 9	(3, 3)	(300, 45)	(300, 26)
Random 10	(3, 3)	(300, 47)	(300, 25)

Data	Layer 1	Layer 2	Layer 3	Layer 4	Layer 5	Layer 6
spiral 1	(2, 2)	(300, 15)	(300, 6)	(300, 7)	(300, 6)	
spiral 2	(2, 2)	(300, 13)	(300, 6)	(300, 7)	(300, 6)	(300, 6)
spiral 3	(2, 2)	(300, 12)	(300, 6)	(300, 7)	(300, 6)	(300, 6)
spiral 4	(2, 2)	(300, 13)	(300, 6)	(300, 7)	(300, 6)	(300, 6)
spiral 5	(2, 2)	(300, 13)	(300, 6)	(300, 7)	(300, 6)	
spiral 6	(2, 2)	(300, 14)	(300, 6)	(300, 7)	(300, 6)	
spiral 7	(2, 2)	(300, 14)	(300, 6)	(300, 7)	(300, 6)	
spiral 8	(2, 2)	(300, 14)	(300, 6)	(300, 7)	(300, 6)	(300, 6)
spiral 9	(2, 2)	(300, 13)	(300, 6)	(300, 7)	(300, 6)	
spiral 10	(2, 2)	(300, 14)	(300, 6)	(300, 7)	(300, 6)	

Data	Layer 1	Layer 2	Layer 3	Layer 4	Layer 5	Layer 6
wine 1	(13, 11)	(300, 76)	(300, 6)	(300, 7)	(300, 6)	(300, 6)
wine 2	(13, 11)	(300, 76)	(300, 6)	(300, 6)	(300, 6)	(300, 6)
wine 3	(13, 11)	(300, 75)	(300, 6)	(300, 7)	(300, 6)	(300, 6)
wine 4	(13, 11)	(300, 76)	(300, 6)	(300, 6)	(300, 6)	(300, 6)
wine 5	(13, 11)	(300, 74)	(300, 6)	(300, 7)	(300, 6)	(300, 6)
wine 6	(13, 11)	(300, 74)	(300, 6)	(300, 6)	(300, 6)	(300, 6)
wine 7	(13, 11)	(300, 74)	(300, 6)	(300, 6)	(300, 6)	(300, 6)
wine 8	(13, 11)	(300, 75)	(300, 6)	(300, 7)	(300, 6)	(300, 6)
wine 9	(13, 11)	(300, 75)	(300, 6)	(300, 8)	(300, 6)	(300, 6)
wine 10	(13, 11)	(300, 76)	(300, 6)	(300, 7)	(300, 6)	(300, 6)

Data	Layer 1	Layer 2	Layer 3	Layer 4	Layer 5	Layer 6
car 1	(6, 6)	(300, 96)	(300, 6)	(300, 8)	(300, 6)	
car 2	(6, 6)	(300, 96)	(300, 6)	(300, 8)	(300, 6)	
car 3	(6, 6)	(300, 91)	(300, 6)	(300, 8)	(300, 6)	
car 4	(6, 6)	(300, 88)	(300, 6)	(300, 8)	(300, 6)	(300, 6)
car 5	(6, 6)	(300, 94)	(300, 6)	(300, 8)	(300, 6)	
car 6	(6, 6)	(300, 93)	(300, 6)	(300, 7)		
car 7	(6, 6)	(300, 92)	(300, 6)	(300, 8)	(300, 6)	
car 8	(6, 6)	(300, 95)	(300, 6)	(300, 7)	(300, 6)	
car 9	(6, 6)	(300, 96)	(300, 6)	(300, 9)	(300, 6)	
car 10	(6, 6)	(300, 99)	(300, 6)	(300, 8)	(300, 6)	

Data	Layer 1	Layer 2	Layer 3	Layer 4	Layer 5
divorce 1	(54, 35)	(300, 44)	(300, 5)	(300, 5)	
divorce 2	(54, 35)	(300, 45)	(300, 4)	(300, 4)	
divorce 3	(54, 36)	(300, 49)	(300, 6)	(300, 6)	
divorce 4	(54, 36)	(300, 47)	(300, 7)	(300, 6)	
divorce 5	(54, 35)	(300, 45)	(300, 6)	(300, 6)	
divorce 6	(54, 36)	(300, 47)	(300, 6)	(300, 6)	
divorce 7	(54, 35)	(300, 45)	(300, 6)	(300, 6)	(300, 4)
divorce 8	(54, 36)	(300, 47)	(300, 6)	(300, 7)	(300, 4)
divorce 9	(54, 36)	(300, 47)	(300, 5)	(300, 5)	
divorce 10	(54, 36)	(300, 47)	(300, 6)	(300, 6)	

Data	Layer 1	Layer 2	Layer 3	Layer 4	Layer 5	Layer 6	Layer 7	Layer 8	Layer 9	Layer 10
cancer 1	(9, 8)	(300, 90)	(300, 5)	(300, 6)	(300, 6)	(300, 5)	(300, 4)	(300, 5)	(300, 6)	(300, 6)
cancer 2	(9, 8)	(300, 90)	(300, 6)	(300, 7)	(300, 8)	(300, 11)	(300, 8)	(300, 4)		
cancer 3	(9, 8)	(300, 88)	(300, 5)	(300, 6)	(300, 7)	(300, 7)	(300, 6)	(300, 4)		
cancer 4	(9, 8)	(300, 93)	(300, 6)	(300, 7)	(300, 9)	(300, 11)	(300, 8)			
cancer 5	(9, 8)	(300, 93)	(300, 9)	(300, 10)	(300, 10)	(300, 11)	(300, 9)	(300, 7)		
cancer 6	(9, 8)	(300, 92)	(300, 7)	(300, 8)	(300, 8)	(300, 7)	(300, 7)			
cancer 7	(9, 8)	(300, 90)	(300, 4)	(300, 4)	(300, 5)	(300, 6)	(300, 6)	(300, 6)	(300, 6)	
cancer 8	(9, 8)	(300, 88)	(300, 5)	(300, 6)	(300, 7)	(300, 8)	(300, 7)	(300, 6)		
cancer 9	(9, 8)	(300, 88)	(300, 5)	(300, 7)	(300, 7)	(300, 7)	(300, 7)			
cancer 10	(9, 8)	(300, 97)	(300, 9)	(300, 11)	(300, 12)	(300, 13)	(300, 6)			

Data	Layer 1	Layer 2	Layer 3	Layer 4
face 1	(960, 233)	(300, 74)	(300, 73)	(300, 46)
face 2	(960, 231)	(300, 75)	(300, 73)	(300, 43)
face 3	(960, 231)	(300, 76)	(300, 73)	(300, 44)
face 4	(960, 232)	(300, 76)	(300, 74)	(300, 44)
face 5	(960, 231)	(300, 77)	(300, 73)	(300, 43)
face 6	(960, 232)	(300, 74)	(300, 72)	(300, 47)
face 7	(960, 232)	(300, 76)	(300, 73)	(300, 45)
face 8	(960, 230)	(300, 74)	(300, 74)	(300, 44)
face 9	(960, 233)	(300, 76)	(300, 76)	(300, 45)
face 10	(960, 231)	(300, 76)	(300, 70)	(300, 43)

Appendix I Sigma Values used for Random and Adversarial Simulation

The simulation of Thm. 1 as shown in Fig. 2 spread the improvement across multiple layers. The σ_l and \mathcal{H}_l values are recorded here. We note that σ_l are reasonably large and not approaching 0 and the improvement of \mathcal{H}_l is monotonic.

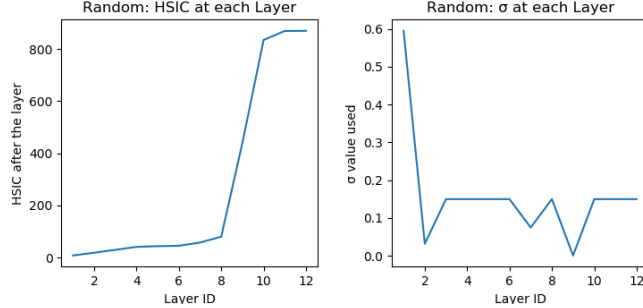


Figure 7

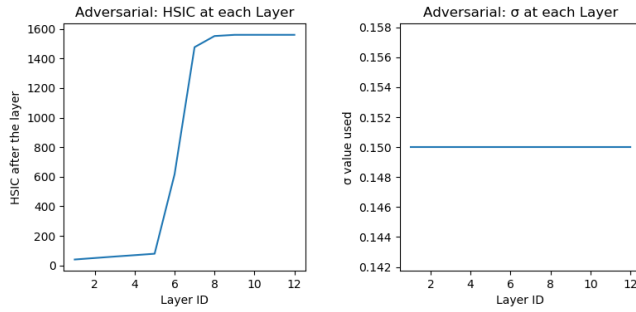


Figure 8

Given a sufficiently small σ_0 and σ_1 , Thm. 1 claims that it can come arbitrarily close to the global optimal using a minimum of 2 layers. We here simulate 2 layers using a relatively small σ values ($\sigma_0 = 10^{-5}$) on the Random (left) and Adversarial (right) data and display the results of the 2 layers below. Notice that given 2 layer, it generated a clearly separable clusters that are pushed far apart.

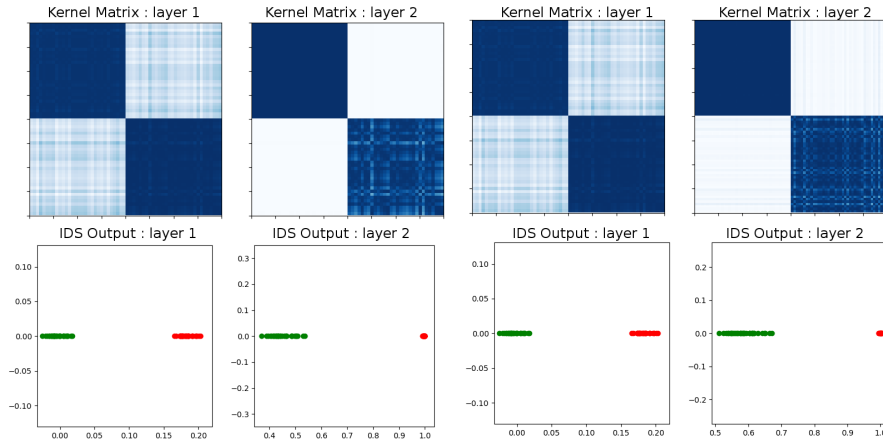


Figure 9: Random Dataset with 2 layers and $\sigma = 10^{-5}$

Figure 10: Adversarial Dataset with 2 layers and $\sigma = 10^{-5}$

Appendix J Graphs of Kernel Sequences

A representation of the *Kernel Sequence* are displayed in the figures below for each dataset. The samples of the kernel matrix are previously organized to form a block structure by placing samples of the same class adjacent to each other. Since the Gaussian kernel is restricted to values between 0 and 1, we let white and dark blue be 0 and 1 respectively where the gradients reflect values in between. Our theorems predict that the *Kernel Sequence* will evolve from an uninformative kernel into a highly discriminating kernel of perfect block structures.

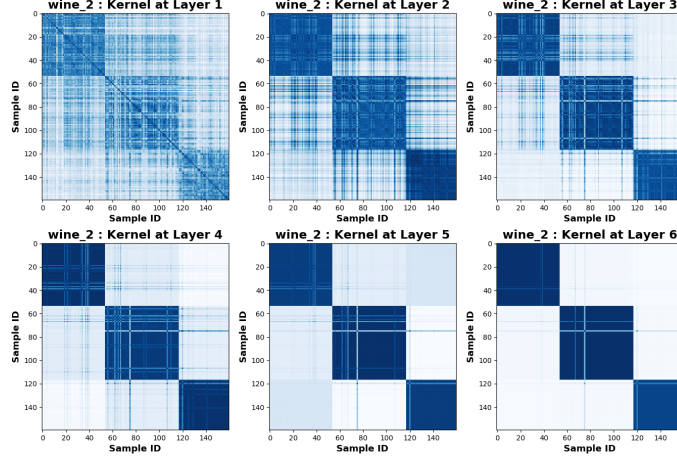


Figure 11: The kernel sequence for the wine dataset.

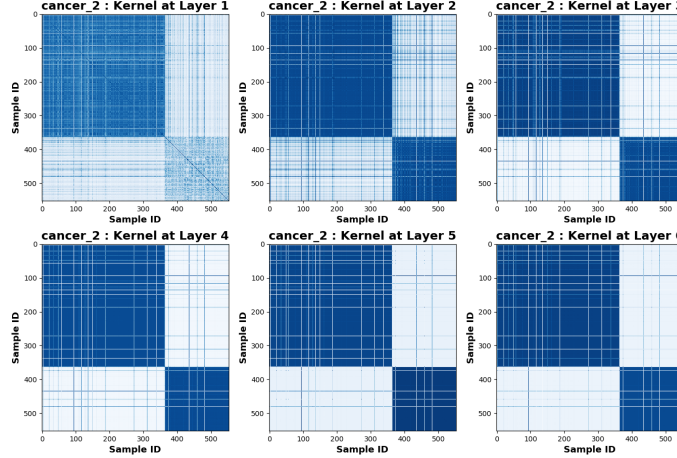


Figure 12: The kernel sequence for the cancer dataset.

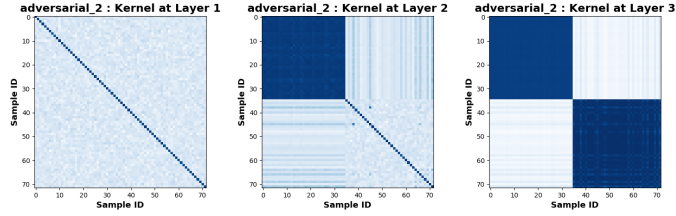


Figure 13: The kernel sequence for the Adversarial dataset.

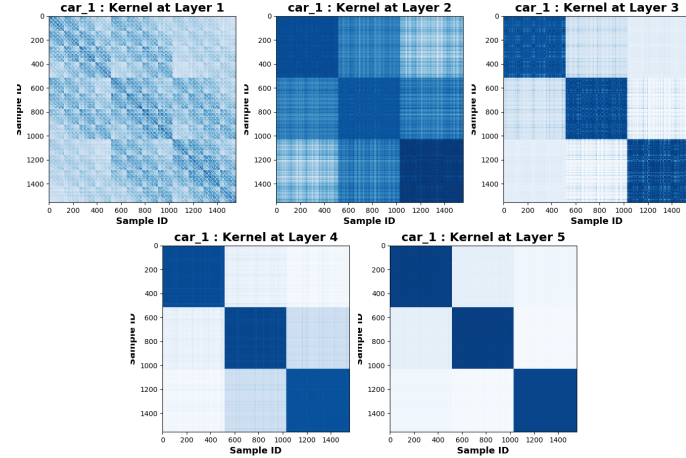


Figure 14: The kernel sequence for the car dataset.

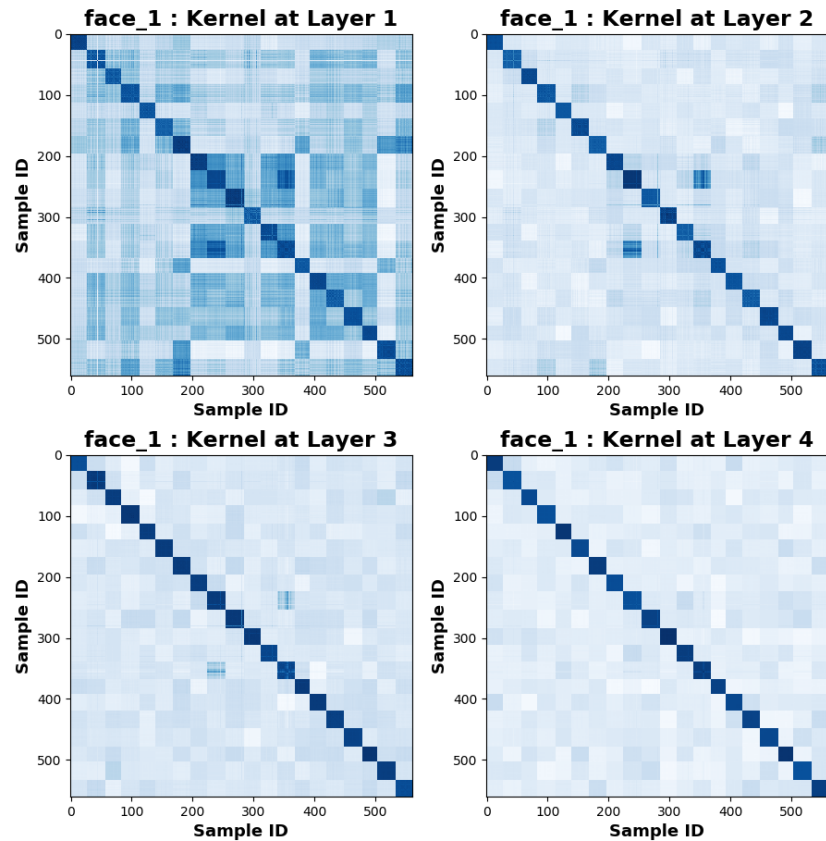


Figure 15: The kernel sequence for the face dataset.

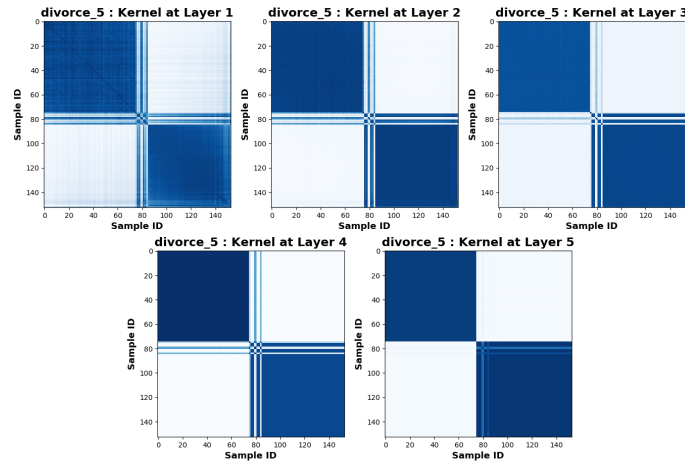


Figure 16: The kernel sequence for the divorce dataset.

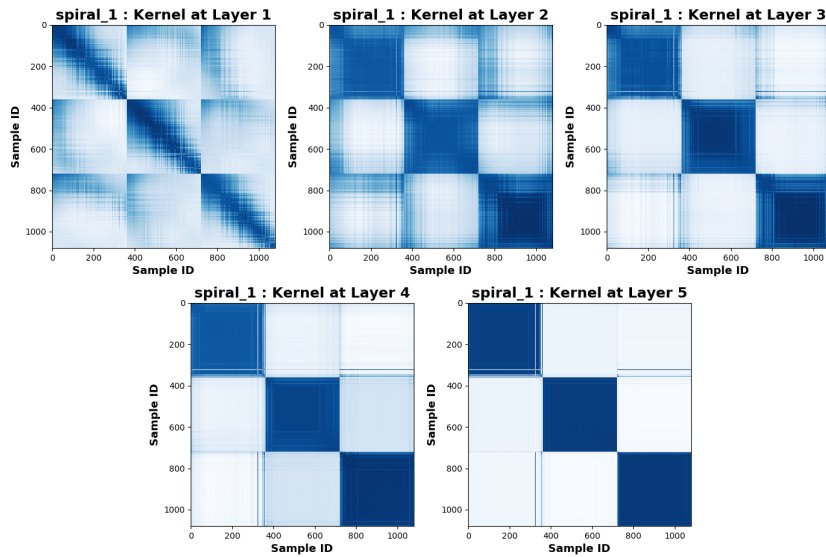


Figure 17: The kernel sequence for the spiral dataset.

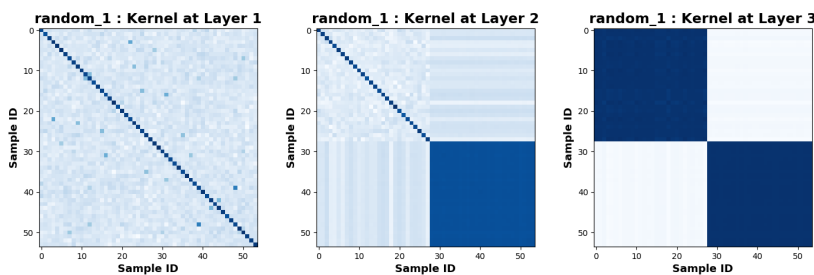


Figure 18: The kernel sequence for the Random dataset.

Appendix K Evaluation Metrics Graphs

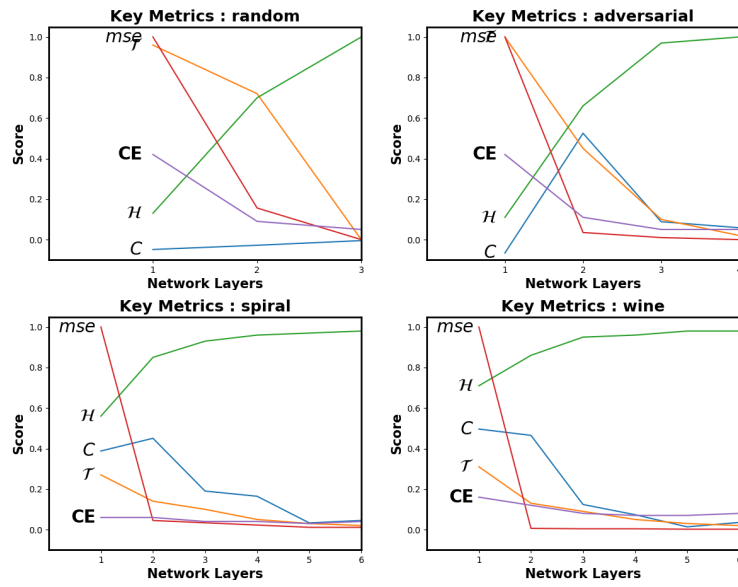


Figure 19

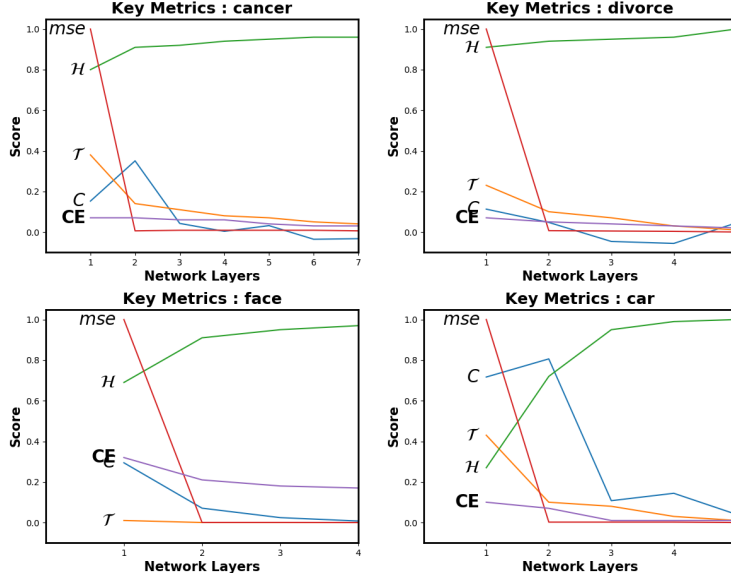


Figure 20: Figures of key metrics for all datasets as samples progress through the network. It is important to notice the uniformly and monotonically increasing \mathcal{H} -Sequence for each plot since this guarantees a converging kernel/risk sequence. As the \mathcal{T} approach 0, samples of the same/difference classes in IDS are being pulled into a single point or pushed maximally apart respectively. As C approach 0, samples of the same/difference classes in RKHS are being pulled into 0 or $\frac{\pi}{2}$ cosine similarity respectively.

Appendix L Optimal Gaussian σ for Maximum Kernel Separation

Although the Gaussian kernel is the most common kernel choice for kernel methods, its σ value is a hyperparameter that must be tuned for each dataset. This work proposes to set the σ value based on the maximum kernel separation. The source code is made publicly available on <https://github.com/anonamous>.

Let $X \in \mathbb{R}^{n \times d}$ be a dataset of n samples with d features and let $Y \in \mathbb{R}^{n \times \tau}$ be the corresponding one-hot encoded labels where τ denotes the number of classes. Given $\kappa_X(\cdot, \cdot)$ and $\kappa_Y(\cdot, \cdot)$ as two kernel functions that applies respectively to X and Y to construct kernel matrices $K_X \in \mathbb{R}^{n \times n}$ and $K_Y \in \mathbb{R}^{n \times n}$. Given a set \mathcal{S} , we denote $|\mathcal{S}|$ as the number of elements within the set. Also let \mathcal{S} and \mathcal{S}^c be sets of all pairs of samples of (x_i, x_j) from a dataset X that belongs to the same and different classes respectively, then the average kernel value for all (x_i, x_j) pairs with the same class is

$$d_{\mathcal{S}} = \frac{1}{|\mathcal{S}|} \sum_{i,j \in \mathcal{S}} e^{-\frac{\|x_i - x_j\|^2}{2\sigma^2}} \quad (183)$$

and the average kernel value for all (x_i, x_j) pairs between different classes is

$$d_{\mathcal{S}^c} = \frac{1}{|\mathcal{S}^c|} \sum_{i,j \in \mathcal{S}^c} e^{-\frac{\|x_i - x_j\|^2}{2\sigma^2}}. \quad (184)$$

We propose to find the σ that maximizes the difference between $d_{\mathcal{S}}$ and $d_{\mathcal{S}^c}$ or

$$\max_{\sigma} \frac{1}{|\mathcal{S}|} \sum_{i,j \in \mathcal{S}} e^{-\frac{\|x_i - x_j\|^2}{2\sigma^2}} - \frac{1}{|\mathcal{S}^c|} \sum_{i,j \in \mathcal{S}^c} e^{-\frac{\|x_i - x_j\|^2}{2\sigma^2}}. \quad (185)$$

It turns out that this expression can be computed efficiently. Let $g = \frac{1}{|\mathcal{S}|}$ and $\bar{g} = \frac{1}{|\mathcal{S}^c|}$, and let $\mathbf{1}_{n \times n} \in \mathbb{R}^{n \times n}$ be a matrix of 1s, then we can define Q as

$$Q = -gK_Y + \bar{g}(\mathbf{1}_{n \times n} - K_Y). \quad (186)$$

Or Q can be written more compactly as

$$Q = \bar{g}\mathbf{1}_{n \times n} - (g + \bar{g})K_Y. \quad (187)$$

Given Q , Eq. (185) becomes

$$\min_{\sigma} \text{Tr}(K_X Q). \quad (188)$$

This objective can be efficiently solved with BFGS.

Below in Fig. 21, we plot out the average within cluster kernel and the between cluster kernel values as we vary σ . From the plot, we can see that the maximum separation is discovered via BFGS.

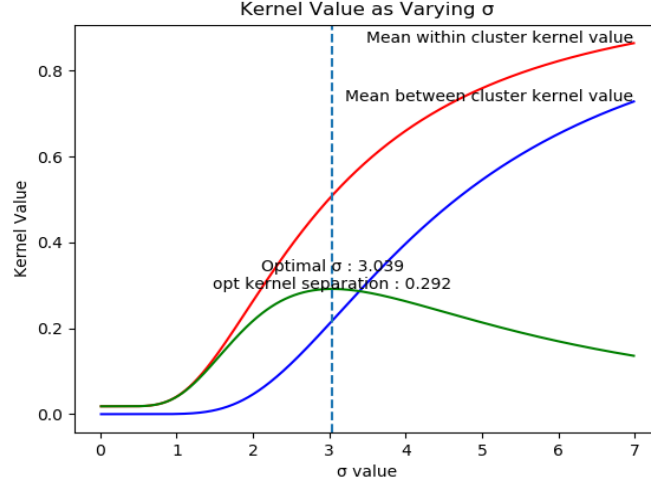


Figure 21: Maximum Kernel separation.

Relation to HSIC. From Eq. (188), we can see that the σ that causes maximum kernel separation is directly related to HSIC. Given that the HSIC objective is normally written as

$$\min_{\sigma} \text{Tr}(K_X H K_Y H), \quad (189)$$

by setting $Q = H K_Y H$, we can see how the two formulations are related. While the maximum kernel separation places the weight of each sample pair equally, HSIC weights the pair differently. We also notice that the $Q_{i,j}$ element is positive/negative for (x_i, x_j) pairs that are with/between classes respectively. Therefore, the argument for the global optimum should be relatively close for both objectives. Below in Figure 22, we show a figure of HSIC values as we vary σ . Notice how the optimal σ is almost equivalent to the solution from maximum kernel separation. For the purpose of $KNet$, we use σ that maximizes the HSIC value.

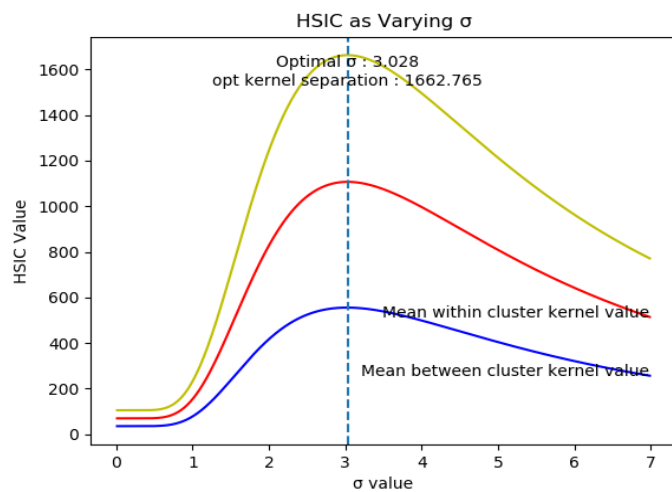


Figure 22: Maximal HSIC.